CHINESE OPTICS LETTERS

Vol. 20, No. 7 | July 2022

Recent advances on perfect light absorbers and their promise for high-performance opto-electronic devices [Invited]

Shu Zong (宗 树)[†], Dongwen Zeng (曾冬文)[†], Wen Yuan (袁 文), Guiqiang Liu (刘桂强)[*], and Zhengqi Liu (刘正奇)[**]

Jiangxi Provincial Key Laboratory of Optoelectronic and Telecommunication, Jiangxi Key Laboratory of Nanomaterials and Sensors, College of Physics and Communication Electronics, Jiangxi Normal University, Nanchang 330022, China

[*]**Corresponding author:** liugq@jxnu.edu.cn

[**]**Corresponding author:** zliu@jxnu.edu.cn

Received February 17, 2022 | Accepted April 24, 2022 | Posted Online May 31, 2022

Perfect absorbers (PAs) are devices that can efficiently absorb electromagnetic waves. Great attention has been attracted since metamaterial PAs (MPAs) were first proposed in 2008. In recent years, with the development of nanophotonics and the improvement of nanomanufacturing technology, considerable progresses have been achieved in designing MPAs using new materials and new structures. In this review, we summarized first the latest developments of PAs from five directions: dual-band, multi-band, wideband, narrow-band, and tunable light absorption. The shortcomings of the previous PAs and the latest improvements were introduced as well. Then, the application of perfect absorption in solar cells, sensors, switches, and structural colors was discussed. Finally, we presented the main challenges and prospects in these fields. Novel PAs for applications in a wide field of opto-electronic devices will continuously progress with breakthrough advances in absorbers related technology and science.

Keywords: perfect absorber; metamaterials; sensor; solar absorption; switch; structural color.

DOI: 10.3788/COL202220.073603

1. Introduction

An electromagnetic wave absorber is a device that can absorb and annihilate electromagnetic waves, which is widely used in various fields of military, science and technology, and people's livelihood. Therefore, the development of perfect absorption and functional devices is always a hot spot in the physics community. Metamaterials are artificially designed structures that exhibit supernormal physical properties not found in natural materials. The resonance excited by its unique geometric structure of united cell enables it to have a strong interaction with electromagnetic fields. The ability makes it widely used in the fields of antenna enhancement[1–3], super lens[4,5], stealth[6,7], etc. In 2008, the first, to the best of our knowledge, metamaterial perfect absorber (MPA) was experimentally demonstrated by Landy *et al.*[8], which could absorb the electric and magnetic field components of the radiation on its surface to a great extent and absorb more than 88% of electromagnetic waves at 11.5 GHz. With the proposal of this idea, in the next 10 years, a large number of metamaterials-based perfect absorbers (PAs) were simulated and manufactured. The absorption frequency of electromagnetic waves has broadened to microwave[9,10], infrared[11,12], visible light[13,14], and terahertz[15,16]. The performance of the MPA has been enhanced because the classic metal-insulator-metal (MIM) structure cannot satisfy our pursuit of a truly near-unity absorption. The absorption modes of MPA have also developed from single-band[17] to dual-band[18], multi-band, broadband[19–22], and tunable features.

In this review, the first part summarizes the latest progress in PAs and introduces five directions of narrow-band, dual-band, multi-band, broadband, and tunable absorption based on the differences in the applications of different absorbers. We summarize the shortcomings of the previous PAs and the latest improvements. In the second part, we introduce the application of perfect absorption in solar cells, sensors, switches, and structural colors. Finally, the main challenges and prospects are discussed.

2. The Latest Development of Perfect Absorbers

The traditional absorbers based on Fabry–Perot (FP) resonance (Fig. 1) have played an indispensable role in the development of MPA, which generally consists of an MIM structure with

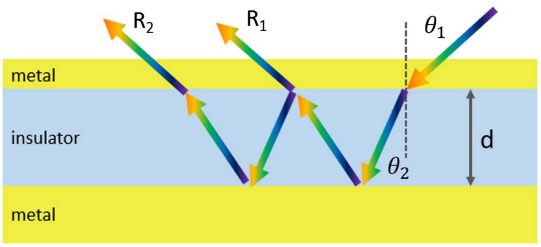

Fig. 1. Schematic of the resonant FP cavity.

multiple layers. The MIM structure is composed of a metal mirror on the top, an insulator in the middle, and a metal bottom plate; for example, the first MPA is composed of a metal ring resonator, a dielectric layer, and a metal wire. For the first MPA, the electrical response is excited by the strong coupling between the metal ring resonator and the incident electric field, and magnetic coupling is achieved by anti-parallel currents between the metal wire and the metal ring resonator center line[23]. Furthermore, based on the principle of impedance matching[24,25], the MPA can minimize the reflection of incident electromagnetic waves. Surface plasmon polaritons on the periodic structure of the top layer can be excited by incident electromagnetic waves, which absorb a large amount of electromagnetic waves. The thickness of the bottom metal plate is greater than the penetration depth of electromagnetic waves, so the electromagnetic waves cannot penetrate the absorber. The device composed of an MIM structure can flexibly change the function of the device and adjust the bandwidth by changing the geometric shape and the thickness of the insulator. However, surface plasmon-based resonance is a kind of resonance with a narrow bandwidth, and, in order to expand the bandwidth, it is necessary to integrate multi-shaped or multi-size resonators in the unitary cell or to stack the resonators in the vertical direction. Device miniaturization is widely pursued, so the above approaches are obviously undesirable. In the specific applications of optical anti-counterfeiting[26,27], color display[28–30], camouflage[31], and heat sink[32], we need a PA that can be tuned. In terms of solar energy absorption, we then need a PA with ultra-broad bandwidth, polarization insensitivity[33], and large incident angle tolerance.

2.1. The latest development of narrow-band perfect absorbers

The first, to the best of our knowledge, perfect metamaterial absorber (MA) proposed by Landy *et al.* is a relative narrow-band absorber[8]. Nonetheless, the absorption bandwidth of this absorber is relatively wide, and the absorption efficiency is not high enough. In practical applications, an absorber that has a narrower bandwidth and higher absorption rate is widely required. Zhang *et al.* proposed an absorption-enhanced resonance structure based on a single-layer molybdenum disulfide subwavelength grating[34]. This absorber includes a molybdenum disulfide grating, a titanium (Ti) dioxide waveguide layer, a silicon substrate layer, and a gold mirror [Fig. 2(a)]. This

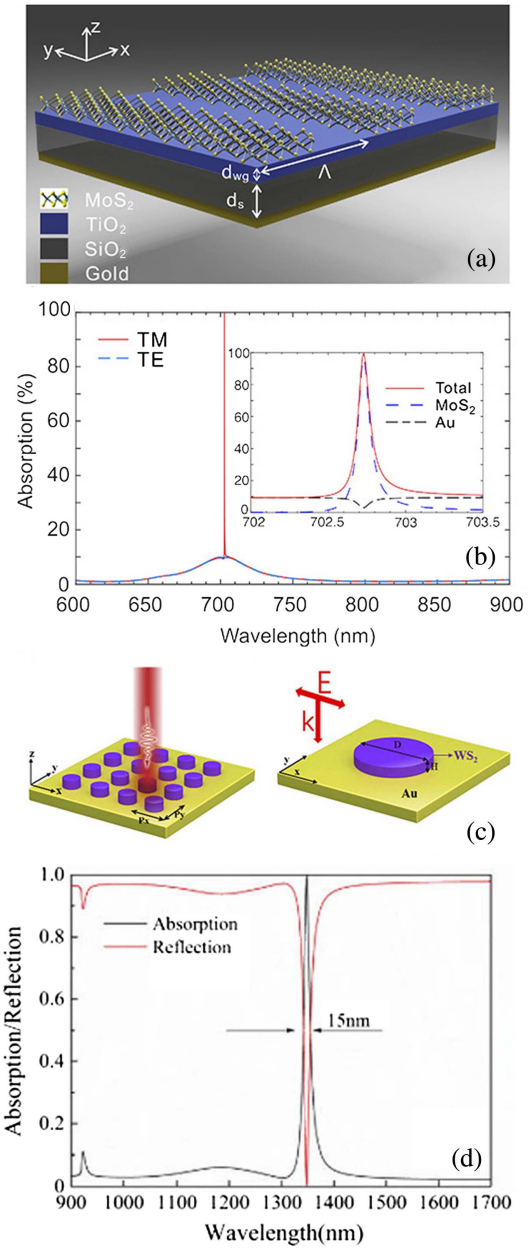

Fig. 2. (a) Schematic of the MoS_2-based PA. (b) Simulated results of the monolayer MoS_2-based PAs[34]. (c) Illustration of the WS_2 MPAs and the unit cell. (d) Absorption and reflection spectra of the MPAs[35].

structure does not require surface plasmon resonance (SPR) or other nanostructured resonances. It only relies on the guided mode resonance (GMR) of molybdenum disulfide, which then achieves an ultra-narrow bandwidth of 0.1 nm for TM polarization with the absorption of 99.71% at 702.73 nm [Fig. 2(b)]. Based on the good design of the parameters, the energy absorbed by the structure is equal to the energy of the molybdenum dioxide coupling into the structure. That is, the critical coupling condition of the structure is reached, making the absorption bandwidth down to 0.1 nm. This parameter is designed for TM polarization. Such a wide and weak peak in the range of 600 to 900 nm depending on the FP effect is obtained under

TE polarization. Li *et al.*[35] proposed a structure in which tungsten disulfide nanodiscs are periodically arranged on a gold film [Fig. 2(c)]. The periodically arranged tungsten disulfide disks can be used to scatter incident light into diffracted waves. These diffracted waves on the plane are called Rayleigh anomalies (RAs). Otherwise, the tungsten disulfide nanodisks can support magnetic dipole (MD) modes[36]. The coupling of RA and MD modes results in the excitation of surface lattice resonance (SLR)[37,38], which can effectively suppress radiation damping and produce a resonance with a high-quality factor (Q factor). This design achieves perfect absorption with a bandwidth of 15 nm and an absorption efficiency of 99.998% [Fig. 2(d)]. Meanwhile, the utilization of novel materials paved another way. Pan *et al.* proposed an ultra-narrow-band absorber with a dielectric-dielectric-metal structure, consisting of Al_2O_3 nanodisk arrays, a SiO_2 dielectric layer, an Au film, and the substrate layer[39]. The simulated outcome shows that the maximum absorption is over 99.7% at 674.7 nm, with an FWHM of 0.45 nm. In this absorber, Al_2O_3 was utilized to construct the antenna layer. The researcher showed calculated results of an absorption of only 11.8% if the absorber was without the Al_2O_3 nanodisks array. It is crucial that Al_2O_3 nanodisks array works in this absorber. This dielectric array not only plays an important role in the absorption of electromagnetic waves but also can effectively trap the light into the SiO_2 layer. The SiO_2 layer is a dielectric resonant cavity that can obtain an ultra-narrow bandwidth by the high-order electrodes resonance and low loss. Based on the same theory of SLR, Hu and his collaborator utilized gallium arsenide (GaAs) to design an MPA[40]. This MPA only has a GaAs cross-shaped resonator array on an opaque copper/silicon substrate. Simulated results show that this absorber can achieve a near-perfect absorption peak with absorption of 99.49% and high-Q factor value of 637 at 2.44 THz. Meanwhile, an FWHM of 3.83 GHz can be obtained. It has great potential in detecting, imaging, and sensing applications.

Compared to the single-band absorber, multi-band light absorption is more desired for high-integration opto-electronic applications due to its multiple resonant absorption bands. In the next section, we will introduce the latest development of dual-band and multi-band PAs.

2.2. The latest development of dual-band and multi-band perfect absorbers

Perfect absorption of dual-band and multi-band spectra is desirable for many applications. Compared with a single absorption peak, multi-band optical absorption is more suitable for highly integrated opto-electronic applications, such as multi-spectral detection[41] and sensing[42]. Recently, the dielectric structure with low loss and other properties has obtained widespread attention[43,44]. Compared with the single plasmon resonance in the metal structure, since the dielectric cavity supports the multi-cavity mode, the multi-spectral optical resonance can be directly obtained. Recently, a dual-band terahertz PA with ultra-high-Q factor was proposed by Yan and co-workers[45]. The PA consists of a gold film and a SiO_2 dielectric diffractive waveguide integrated on the gold film, which is different from the previous MIM structure. In the MIM structure, the absorption bandwidth is difficult to be very small due to the strong radiation damping and inherent metal loss[46–48]. In order to suppress absorption loss caused by the basic structure, graphene is often used as a substitute for the upper metal part in the MIM structure to reduce loss because of its unique physical properties[49,50]. The graphene structure absorber is based on SPR, which can only achieve a series of single-peak perfect absorption. Two traditional methods were typically used to obtain double peaks or multiple peaks. One method is to utilize complex graphene structures in periodic structures[51], and the other is to superimpose graphene structures and use appropriate methods to separate them[52]. A graphene MPA [Fig. 3(a)] was designed by Li and co-workers[53]. The simulation results show absorption peaks at 48.49 μm and 65.33 μm with the absorption rates of 99.31% and 99.91% [Fig. 3(b)]. In addition, the researchers found that the structure is insensitive to polarization and still has nearly perfect double-band absorption at large angles of incidence. However, absorbers based on these two methods have complex structures and require very high-precision manufacturing processes.

As early as 2016, Liu *et al.*[54] demonstrated a multi-band perfect light absorber (MLPA) based on the coupling of a three-layer dielectric metamaterial structure and a metal substrate [Fig. 4(a)]. The simulation results show that the structure has four absorption peaks. The absorbances at wavelengths of 486.2 nm (λ_1), 492.2 nm (λ_2), 563.3 nm (λ_3), and 628.5 nm

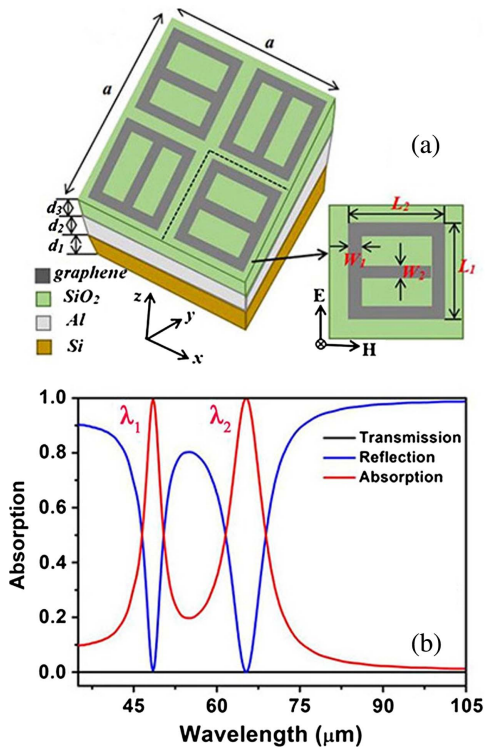

Fig. 3. (a) Schematic of the graphene MPA and the unit cell. (b) Absorption, transmission, and reflection spectra of the graphene MPA[53].

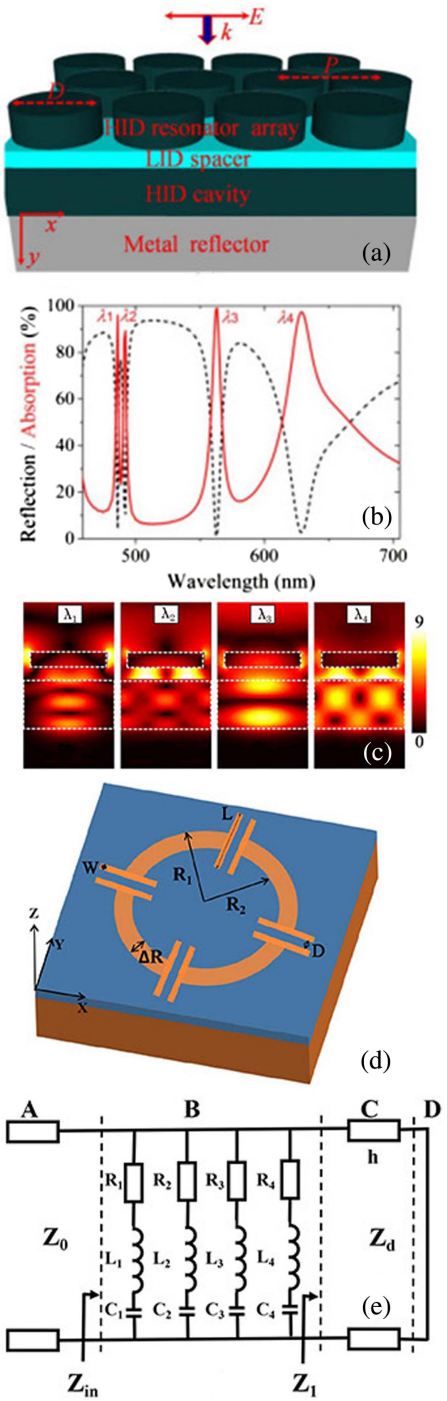

Fig. 4. (a) Schematic of the MLPA. (b) Reflection and absorption spectra of the structure. (c) Normalized electric field intensity distributions of the absorption peaks at λ_1–λ_4, respectively[54]. (d) Illustration of the MPAs. (e) The equivalent circuit model of the absorber[55].

(λ_4) are 95.9%, 89.2%, 98.9%, and 97.3%, respectively [Fig. 4(b)]. Among them, λ_1 and λ_3 are excited by the dipolar resonance generated by the top resonator. λ_2 is generated by the coupling of dipole resonance and cavity mode and its hybrid effect, and λ_4 is excited by the lattice resonance [Fig. 4(c)]. The high symmetry of the structure makes the absorber insensitive to polarization and angle of incidence. Recently, Wang *et al.*[55] theoretically proposed a tri-band absorber composed of a copper-based periodic split ring array-dielectric-copper three-layer film nanostructure [Fig. 4(d)]. The structure has three peaks at $\lambda_1 = 872.54$ nm, $\lambda_2 = 1008.69$ nm, and $\lambda_3 = 1138.62$ nm with the absorption of 87.1%, 99.9%, and 99.6%, respectively. The absorbance, reflectance, and transmittance of the absorber can be expressed as $A(\omega) = 1 - R(\omega) - T(\omega)$. Since the metal bottom plate is thick enough to neglect electromagnetic waves, the formula can be written as $A(\omega) = 1 - R(\omega)$. Based on equivalent circuit analysis [Fig. 4(e)],

$$A(\omega) = 1 - R(\omega) = 1 - \left| \frac{Z_{\text{in}}(\omega) - Z_0}{Z_{\text{in}}(\omega) + Z_0} \right|^2, \tag{1}$$

$$Z_{\text{in}} = \frac{1}{Z_m(\omega)} + \frac{1}{Z_d(\omega)}, \tag{2}$$

$$Z_m(\omega) = \frac{1}{R_1 + j\omega L_1 + \frac{1}{j\omega C_1}} + \frac{1}{R_2 + j\omega L_2 + \frac{1}{j\omega C_2}} + \frac{1}{R_3 + j\omega L_3 + \frac{1}{j\omega C_3}} + \frac{1}{R_4 + j\omega L_4 + \frac{1}{j\omega C_4}}, \tag{3}$$

$$Z_d(\omega) = j\sqrt{\frac{\omega_r \omega_0}{\varepsilon_r \varepsilon_0}} \tan(kh), \tag{4}$$

$$k = \frac{k_0}{\sqrt{\varepsilon_r \omega_r}}, \tag{5}$$

where ω_0, k, and ε_r, respectively, represent permeability, wavenumber, and relative permittivity of the dielectric layer. ω_0, k_0, and ε_0 are permeability, wavenumber, and relative permittivity of free space. Z_{in} and Z_0 are the input impedance of the MPA and the impedance of free space, respectively. When Z_{in} is equal to Z_0, MPA can achieve perfect absorption. Graphene-based MAs are widely used in single-band absorption[56]. Recently, researchers have combined graphene plasma with an MPA using the better field confinement and lower dispersion loss of graphene plasma to achieve perfect absorption in nine bands[57]. This absorber structure includes an out-of-plane metal-insulator-graphene (MIG) heterostructure composed of Ag, ZnS, and graphene, a SiO_2 spacer, and a metal substrate. When the surface plasmon polaritons (SPPs) of graphene are excited, they will bounce back and forth between fields to the two abrupt edges, realizing normal standing-wave resonance on the individual graphene ribbon. The simulation results show that all incident power is trapped in the MIG gap without any transmission or reflection, which leads to near-unity absorption. The bandwidth of MPA is not broad enough in the previous reports, whether it is a single-band absorber or a multi-band absorber. It inevitably limits the application fields of MPA.

2.3. The latest development of ultra-wideband perfect absorbers

The technologies of broadband spectral absorption from visible light to infrared light have gained a lot of attention, due to its

applications related to energy[58–61] and sensing[62–64] in the past 10 years. The realization of perfect absorption in a wide spectral band has a positive role in promoting the development of thermal emission[65–67], perfect stealth[68–71], infrared imaging[72–76], radiation cooling[77,78], and other applications[79]. There are many ways to achieve wide-wavelength absorption, for example, metal grating[80–83], photonic crystal[84–86], nanocomposite material[87–90], quasi-periodic nanocone[91], graphene resonators[92,93], and nanorings[94].

A disordered gold nanoparticles multilayer structure absorber was proposed, which was deposited on a $Ge_2Sb_2Te_5$ chalcogenide thin film by one-step self-assembly of gold nanoparticle clusters[95]. The entire absorber was placed on a silicon substrate. Due to coalescence of the dielectric layer and high-density localized SPR (LSPR) modes induced by randomly distributed gold nanoparticles, the absorber achieves 92% absorptivity and polarization insensitivity in the spectral range from 400 nm to 1000 nm[96–98]. Similarly, an absorber constructed by combining gold nanoparticles with MXene takes advantage of the broadband absorption and tunable energy bandgap of MXene (transition metal carbides, nitrides, or carbonitrides)[99]. Based on plasmonic resonance, magnetic resonance, and cavity effects, the absorber achieves polarization-insensitive and angle-independent perfect absorption (up to 99% absorption rate) in the ultraviolet (UV) to infrared band. In general, particle-based plasmonic nanostructures can be fabricated by electrochemical deposition, self-assembly, dealloying, and sputtering on porous templates. Similar nanoparticle absorbers exhibit extremely high scalability, spectral applicability, and utility. Nonethless, absorbers with disordered nanoparticle structures are generally only available on a few specific material platforms, such as silicon. In addition, some nanoparticles have relatively low melting points, which also limit their application in opto-electronic and photovoltaic devices. Lately, Chang *et al.* experimentally demonstrate the realization of a broadband absorber by coating Ti nitride on disordered anodic aluminum (Al) oxide (AAO) nanotemplate[100]. Disordered pores were etched on the AAO nanotemplate by wet etching [Fig. 5(a)]. A Ti nitride layer was then coated on the AAO by atomic-layer deposition[101–103]. The absorber achieves perfect polarization-insensitive and angle-independent absorption at visible and near-infrared wavelengths, with more than 95% absorption at visible wavelengths. The absorber has the advantages of low cost and good heat resistance and provides an effective solution for large-scale applications[104]. In this regard, a broadband light absorber [Fig. 5(b)] with nanostructured super-surfaces directly located on the thin absorption layer of commercial thermoelectric devices was designed by Nityan *et al.*[105]. It can be applied to the range of visible light to short-wave infrared. The absorption structure consists of an MIM multilayer, which can be fabricated via the focused ion beam (FIB) to create nanostructures directly on the polished surface of the device. The absorber can be applied in the visible to short-wave infrared (350–2600 nm) range and achieves an extinction peak at ~495 nm [Fig. 5(c)]. In addition, the simulated absorption spectra of a planar thin film, nanostructure, and planar rough nanostructure are compared in Fig. 5(d). It can be seen that the absorbance of the planar thin film is very low, while the nanostructure has a strong absorption peak at short-wave infrared (1550 nm) and two absorption peaks in the visible range. The absorption by planar rough nanostructures can cover the range of visible light to short-wave infrared, but the absorption rate decreases gradually with the increase of wavelength due to the diffuse reflection. A PA means that both transmission and reflection are close to zero.

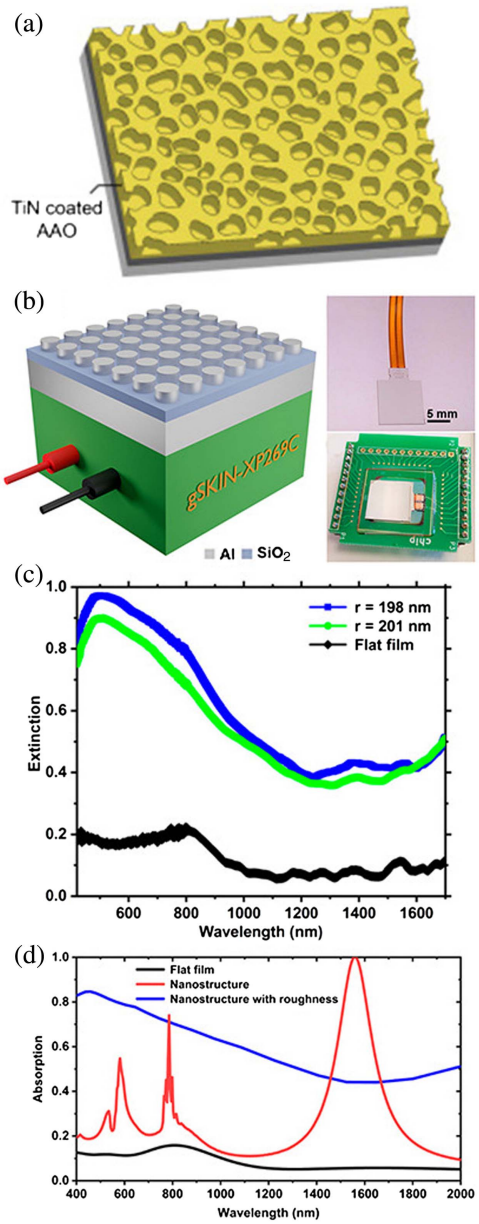

Fig. 5. (a) Schematic of broadband titanium nitride disordered MAs[100]. (b) Schematic of a nanostructured wideband light absorber prepared on top of a commercial thermoelectric device. (c) The extinction spectra of the flat film and two nanostructures with radius of $r = 198$ nm and 201 nm are measured in the visible and short-wave infrared regions. (d) Extinction spectra of the flat film, nanostructure, and nanostructure with surface roughness are simulated[105].

When the impedance of the absorbing layer matches that of free space, zero reflection can be achieved. For the purpose of zero transmission, the selection of the thick enough bottom metal film to block transmission completely is usually easy to be realized. The hybrid device shows a linear response, and the response time is an order of magnitude higher than that of flat metal films, so the absorber has a significant advantage in realizing a new generation of thermal photodetectors.

It is innovative for the wideband absorber to integrate into commercial thermoelectric devices. Nevertheless, a critical problem is that although the bandwidth of the absorber meets the requirements, the average absorption rate over the whole broadband range is not high.

In recent years, metal grating MAs have attracted much attention because of their simple and cost-effective design. Cai *et al.*[106] proposed and designed a double-layer grating ultra-wideband MA using rigorous coupled wave analysis (RCWA) and genetic algorithm (GA)[107]. As shown in the Fig. 6(a), the top of the absorber is a SiO_2-Ti square double-layer grating, which acts as an anti-reflection and induced resonance to enhance light absorption. There is a SiO_2 dielectric layer under the double grating for magnetic resonance excitation and then the Ti bottom layer as the substrate of non-precious metal. The average absorptivity in the wavelength range of 300–2100 nm is 98.3%, especially in the wavelength range of 545–635 nm and 1371–1822 nm, achieving extremely high absorptivity (absorptivity > 99%) [Fig. 6(b)]. In addition, the symmetrical MA is independent of polarization and insensitive to incident angles of TM and TE polarized waves[108], which has been widely used in the field of solar energy. Structures composed of alternating layers of metal and dielectric provide the widest absorption bandwidth to date[109–112], but face a trade-off between optical performance and material selection with those structures with the widest bandwidth using only CMOS-incompatible materials hindering their large-scale application[113]. By carefully studying the unique properties of Al and zinc sulfide materials, both materials are CMOS compatible. Yue *et al.*[77] proposed zigzag and pyramidal multilayer absorbers [Fig. 6(c)] with operating bandwidths (0.2–15 μm) ranging from UV to long-wave infrared (LWIR), while being compatible with CMOS technology. As can be seen from Fig. 6(d), the average absorptivity of TM polarized light (black curve) is greater than 90% in the wavelength range of 1–5 μm and close to 100% in the wavelength range of 8–14 μm (green background). Based on these characteristics, the multilayer absorber has potential applications in infrared imaging and spectroscopy, radiation cooling, solar energy conversion, and so on.

In addition, we sorted out a table of absorption efficiency of light absorbers of various materials by comprehensively reviewing literatures on broadband light absorption in the past two years, as shown in Table 1.

2.4. Recent advances in tunable perfect absorbers

Achieving controllable and compact perfect absorption has great prospects in nanophotonic systems. However, most of the

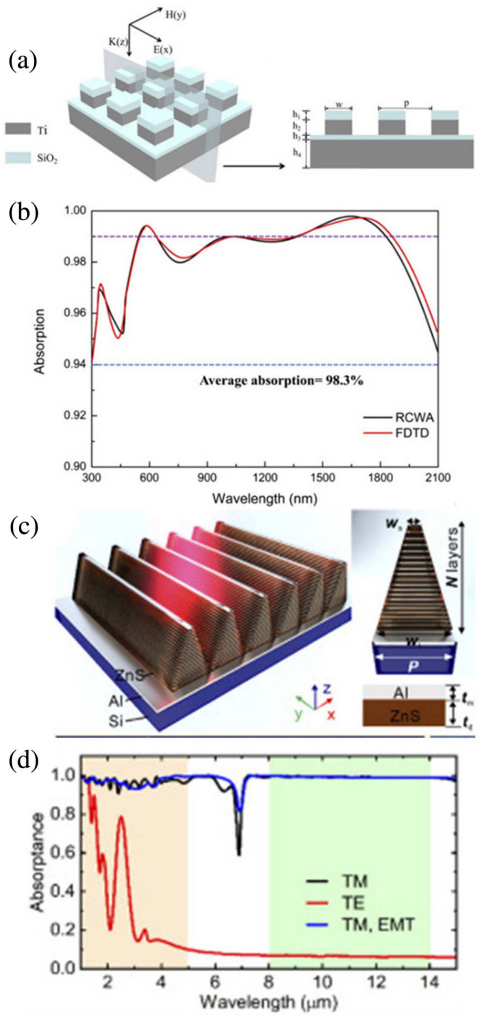

Fig. 6. (a) Schematic of the absorber and the corresponding cross-section view. (b) The absorption spectra of the MA with optimized geometry[106]. (c) Schematic diagram of Al-ZnS multilayer sawtooth absorber and a single structural unit. (d) The absorption spectra of TM and TE polarized light incidence and hyperbolic metamaterials with TM polarized light incidence under effective medium theory are studied[77].

absorbers reported in recent years were focused on metal or lossy media, leading to the lack of structural and behavior flexibility. The absorption properties are fixed and cannot be adjusted in a controllable way[123–127]. Han *et al.*[128] proposed an independently tunable multipurpose monolayer graphene MA (GMA) at mid-infrared wavelengths [Figs. 7(a) and 7(b)]. The simulation results show that the structure has two perfect absorption peaks. By changing the Fermi level of graphene under the resonator to change the resonant frequency, each absorption peak can achieve a high absorption rate of 99% [Figs. 7(c) and 7(d)]. Under oblique illumination, the absorber retains the high absorption over a wide range of angles. In addition, multi-band and wideband absorption can be observed by increasing the number of resonators in the unit cell and adjusting their size.

Table 1. Comparison of Representative Theoretical and Experimental Works on the Topic of Ultra-Broadband MPAs in Recent Years.

Work by	Device Configuration	Bandwidth	Absorptance	Reference
Chen *et al.* (2021)	MgF_2 and Cr	900–1900 nm	> 90%	[114]
Cai *et al.* (2020)	SiO_2 film and Ti substrate	300–2100 nm	98.3%	[106]
Yue *et al.* (2020)	Al and ZnS	0.2–15 μm (UV-LWIR)	Angle of 50° > 90%, angle of 60° > 80%	[77]
Liu *et al.* (2020)	Si, Ti, MgF_2, and Al	405–1505 nm (vis-to-NIR)	95.14%	[69]
Zhang *et al.* (2020)	TiN/TiO_2	0.5–1.8 μm (vis-to-NIR)	95.6%	[65]
Ijaz *et al.* (2021)	ZrN	400–800 nm 280–2200 nm	> 95% > 86%	[66]
Zhao *et al.* (2020)	Ge and SiO_2	450–750 nm (vis)	97.4%	[115]
Dong *et al.* (2021)	ITO and HfO_2	300–1000 nm	Average 96%, maximum > 99%	[116]
Zhong *et al.* (2021)	Ti	0.38–2.0 μm (vis-to-NIR)	Average 93.6%, maximum 98.9%	[117]
Guo *et al.* (2021)	TiN	100–2500 nm (vis-to-NIR)	Average 96.11%	[118]
Zhou *et al.* (2021)	Ti and Si (MIM)	400–2500 nm (vis-to-NIR)	Average 93.8%, maximum 99.8%	[119]
Qian *et al.* (2021)	SiO_2, Si, Cr, and Al	400–1800 nm	96.1%	[120]
Piao *et al.* (2021)	TiN	300–2500 nm	> 99%	[121]
Zhang *et al.* (2020)	W and SiO_2	300–1200 nm	TE: average 96%, maximum 99.4%; TM: average 91%, maximum 99.8%	[122]

Although these absorbers based on van der Waals (VDW) materials can be tuned, their operating bandwidth is limited. It is troublesome to utilize the absorber because graphene always requires an external electrical bias[129–131]. Phase change material (PCM) is an active functional material that can change its phase in response to external stimuli[132]. Among these PCMs, vanadium dioxide (VO_2) exhibits a good transition behavior from insulator phase to metal phase at about 340 K[133], and its conductivity changes significantly with temperature[134–136]. Hexagonal boron nitride (hBN) and PCM VO_2[137,138] were used to fabricate MPA [Fig. 7(e)]. After stacking VO_2 and hBN layers, the spectral position of the absorption peak can be dynamically switched by changing the temperature. When the temperature is higher than the critical temperature ($T_c = 68$°C), the plasmon resonance of the PCM VO_2 can produce an absorption peak at 12 μm. Another absorption peak can be generated at 7.2 μm [Fig. 7(f)] when the temperature is lower than the critical temperature. Due to the phonon polarization of the hyperbolic material hBN, both absorption peaks can reach about 100%. At the same time, by studying the dependence of the absorption on the polarization angle and the incident angle, the flexibility of the absorber is proved. The researchers' findings open new possibilities for many multi-functional minimization applications, such as optical modulators[139], optical switches[140], and temperature control systems. Similarly, based on the remarkable tunability and compatibility of the optical properties of the PCM VO_2, a dynamically tunable absorber (DTA) was designed[141] by integrating a thin film of VO_2 into an MIM structure metasurface absorber [Fig. 7(g)]. By controlling the temperature of the VO_2 insulator-metal phase transition and the FP resonance of the absorber, the dynamically adjustable absorber can achieve a new switching function in the full visible light band (400–780 nm) [Fig. 7(h)]. The results show that DTA has potential application value in the optical control field in the visible light range.

3. Application of the Perfect Absorber

In the past decade, MPA showed notable and excellent property and emerged with extensive applications[142–144]. In this part, we will introduce the application of MPA in solar energy harvesting, sensors, switches, and structural colors, and its advantages and disadvantages. In the field of solar energy harvesting, MPA can be utilized for solar cells and seawater evaporation and desalination. It is remarkable that MPA has an extensive absorption band in the visible and infrared range, and the absorption of MPA can be up to 99%. However, most MPAs are artificially

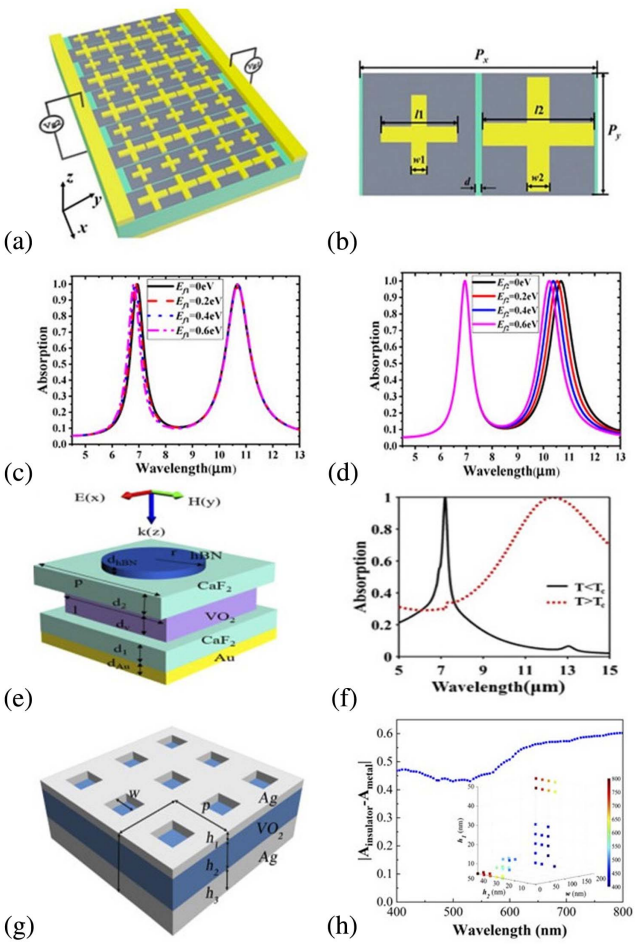

Fig. 7. (a) Illustration of an independent tunable multipurpose absorber using a monolayer metal-graphene metamaterial. (b) Top view of a single structural unit. (c) Absorption spectra obtained by E_{f1} independently. (d) Absorption spectra obtained by E_{f2} independently[128]. (e) Schematic diagram of polarized light incident into the absorber structural unit. (f) Absorption of $T < T_c$ and $T > T_c$ is simulated, respectively[137]. (g) The proposed 3D schematic diagram of DTA based on VO_2. (h) Absorption contrast of each characteristic wavelength is calculated when the structural parameters are w = 0–200 nm, h_1 = 0–100 nm, h_2 = 5–100 nm, h_3 = 200 nm, and p = 200 nm. The device structure parameters corresponding to each characteristic wavelength are shown in the inset[141].

engineered periodic subwavelength nanostructures, which require expensive photolithography. The technology of chemical synthesis, surface dewetting, and self-assembly will be utilized to construct disorder MPA that can effectively reduce cost. Compared with electromagnetic sensors, optical sensors adapt to harsher environments, and sensors based on MPA have significant sensitivity (S). Optical switches and structural colors also show more outstanding practicality and have more outstanding performance than traditional devices.

3.1. Solar energy harvesting

Solar energy, as a kind of clean and renewable energy, has been a popular research object because of its wide application. Solar cells[145–148], photovoltaic devices[149–152], photothermal emitters[153–157], seawater desalination[158–161], and infrared biomedical sterilization[162,163] are some of the most promising applications.

In recent years, the classic MIM structure of the absorber for its perfect absorption also is often used in solar cells. However, this film stack PA mainly absorbs light into two layers of metal heat (ohmic losses), lacking the ability to make solar energy directly from the light into an electric current[164–166]. For this reason, Yang *et al.*[167] proposed a three-layer metal-semiconductor-metal (MSM) cavity based on amorphous silicon (α-Si) and metal thin films. Ag is used as the boundary layer on the top. The thickness is reduced to a few nanometers ($\lambda/100$), and the thickness of the intermediate layer (α-Si layer) is also reduced to the deep subwavelength scale ($\lambda/20 - \lambda/10$). The absorber is not sensitive to TM and TE polarization and incident angle. With the increase of the thickness of the top layer and the middle layer, the position will be redshifted while the absorption rate decreases. Compared with the conventional MIM structure, most of the light absorption (89%) of MSM occurs in the α-Si layer based on the strong resonance trapping of the FP cavity. The use of externally biased devices enables photoelectric conversion of the trapped light for solar cells and photovoltaics, not just the ohmic losses of the MIM metal layers. So, the absorber with this structure is very promising in solar cells and photovoltaic power generation. Nonetheless, the efficiency of solar cells is also limited when the thickness of the silicon layer decreases.

Therefore, light capture has become one of the main topics of thin film solar cells. GaAs has become a good competitor in recent years due to its unique optical properties and high conversion efficiency[168–170]. Li *et al.*[67] proposed a solar absorber based on GaAs nanoantennas, where one-dimensional GaAs nanoantennas were arranged periodically. Each GaAs nanoantenna was coated with a layer of indium tin oxide (ITO), and then the whole GaAs nanoantenna was placed on a thin W-GaAs-Ti three-layer membrane structure [Fig. 8(a)]. Due to the combination of GMR and cavity resonance with SPPs[171], the solar absorber presents an ultra-wide absorption band spanning the visible and mid-infrared regions; bandwidths with absorptivity of more than 90% are greater than 2400 nm [Fig. 8(b)]. The absorber also has good insensitivity to the angle and polarization of incident light. In addition, high short-circuit current density as high as 61.947 mA/cm^2 can be achieved under AM 1.5 sunlight illumination [Figs. 8(c) and 8(d)]. This opens up new paths for ultra-compact and efficient photovoltaic cells[145] and heat emitters[153].

Freshwater is indispensable to human daily life, but the freshwater resources on earth are very limited. Solving the clean water crisis is an important challenge for human sustainable development. During the study of MPA, the researchers found that the light energy absorbed by the MPA was converted into heat energy due to the ohmic loss of the metal and dielectric loss. Based on this photothermal conversion phenomenon, in the field of perfect solar energy absorption, many efforts have been made to realize high-performance absorbers that can drive

seawater evaporation and desalination. Among many metamaterials to achieve perfect broadband absorption, nanocone structured absorbers have attracted attention because of their ease of manufacture and simple principle of achieving broadband absorption.

Wang *et al.*[172] optimized solar energy acquisition and thermal conversion using nanocone structure absorbers [Fig. 9(a)]. It is found that the material, geometric parameters, and shape of the nanocones have a certain influence on the solar energy absorption performance. The results show that the nanocones made of chromium (Cr), nickel (Ni), platinum (Pt), Ti, bismuth telluride (Bi_2Te_3) can complete the perfect solar energy absorption. Based on the gradient index effect and slow-light effect, the optimized absorber has near-perfect absorption performance in the wide wavelength range of 300–2400 nm [Fig. 9(b)], which is suitable for solar energy collection. Although the absorption characteristics of the nanocone absorber are independent of the polarization of light, the small deviation of the incident angle significantly affects the absorption efficiency of the nanocone absorber. Zhong *et al.*[117] selected randomly distributed Ti spheres in the hydrogel layer to achieve perfect ultra-wideband absorption. Utilizing the plasmonic particle resonance of Ti spheres, in-plane plasmonic near-field coupling, and the spatial location of adjacent particles[173], an average absorption rate of 93.6% in the visible to near-infrared range (0.38–2.0 μm) can be realized, with a bandwidth of 1386 nm with an absorption rate above 90% and a maximum absorption of 98.9% due to the absence of a metal reflector. In addition, its absorption is insensitive to both polarization and incident angle. Hyperspectral absorption can be achieved over a wide range of structural parameters. Its absorption characteristics and simple structure provide a new application scheme for solar thermal steam generation and seawater desalination. Compared with the bandwidth and absorption rate, the absorber with complex and precise structure is better than the absorber with disordered structure. But, in large-scale applications, we have to consider the cost issue. MPAs constructed using methods such as chemical synthesis and surface dewetting have advantages over using photolithography[174].

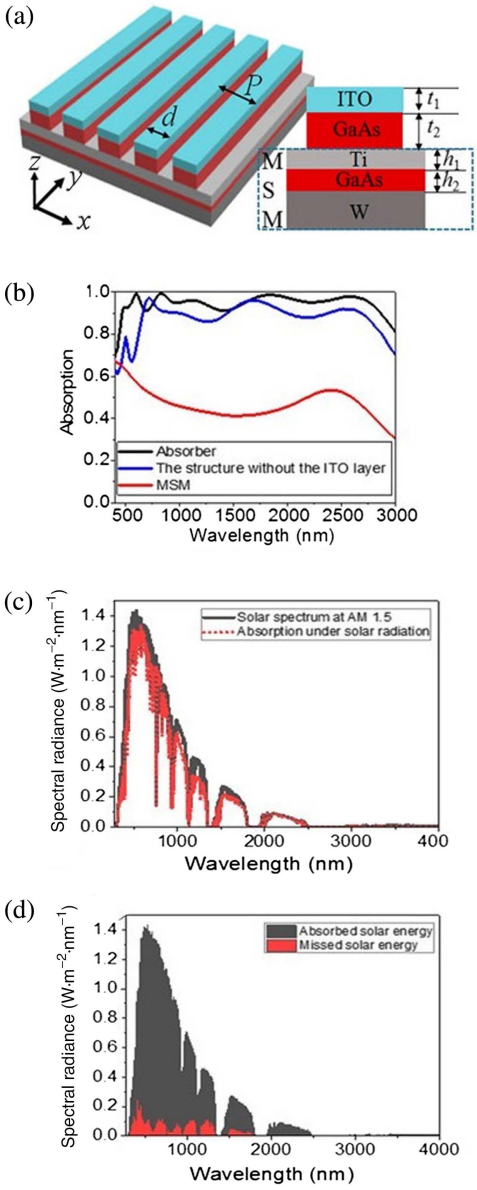

Fig. 8. (a) Schematic and section in 3D of the solar absorber designed. (b) Absorption spectra of the solar absorber, MSM structure, and MSM structure without the ITO layer. (c) Standard spectrum and absorption spectrum of the solar absorber at AM 1.5. (d) Solar energy absorption and leakage in the full spectrum of solar energy[67].

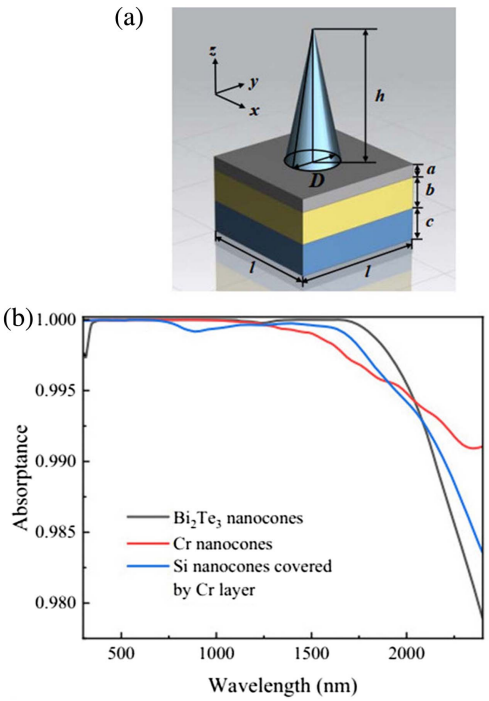

Fig. 9. (a) Basic unit and structural parameters of the absorber. (b) Absorption of the nanocones composed of Bi_2Te_3, Cr, Si, and Si covered with Cr layer, respectively[172].

3.2. Sensors

Sensor is a device that can feel the specified measurement and convert it into usable signals according to certain rules. It is used to obtain information that cannot be directly obtained by human senses. It is widely used in industrial production[175,176], space development[177,178], ocean exploration[179,180], medical diagnosis[181,182], and biological engineering[183,184]. Traditional electrical sensors convert physical phenomena into electrical signals and then adjust them through data acquisition systems. But, they are greatly limited in electromagnetic interference, high-pressure environments, and spaces where traditional sensors are limited. Optical sensors can solve each of these problems, so the development of optical sensors has attracted great attentions. This section mainly introduces a refractive index (RI) sensor based on SPPs. Since the characteristics of the SPPs depend very much on the RI of the adjacent medium. The change of the surrounding environment can cause the change of the resonance wavelength of the SPPs. Therefore, the structure based on SPPs is very suitable for RI sensing and has high S in RI detection. In order to evaluate the performance of the sensor, three measurements are commonly used: the S, figure of merit (FOM), and FOM* defined, as the following:

$$S = \frac{\Delta\lambda}{\Delta n}, \tag{6}$$

$$\mathrm{FOM} = \frac{S}{\mathrm{FWHM}}, \tag{7}$$

$$\mathrm{FOM}^* = \max\left|\frac{\mathrm{d}I(\lambda)/\mathrm{d}n(\lambda)}{I(\lambda)}\right|. \tag{8}$$

$\Delta\lambda$ corresponds to the change in the resonant wavelength when the RI of the medium changes Δn, and FWHM represents the full width at half-maximum of the resonant peak. $\mathrm{d}I(\lambda)/I(\lambda)$ is the relative intensity change at a fixed wavelength induced by an RI change $\mathrm{d}n$. $I(\lambda)$ corresponds to the intensity where FOM* reaches a maximum value. The RI optical sensor based on a plasma absorber was first reported by Liu *et al.* in 2010[185]. Liu *et al.* demonstrated an MIM plasma absorber with a structure consisting of a gold disk array, dielectric layers, and a gold reflector. Its performance is much higher than that of plasmonic nanorods in water, and the S is about 400 nm/RIU. Shen *et al.* recently proposed a method to effectively improve S and FOM using the combination of SPR and Fano resonance[186–188]. The sensor structure made by this method includes a nanoarray and an FP resonator. Since the LSPR of the nanoarray has a wide resonant line shape (regarded as a continuous state), the FP resonator cavity can be indirectly excited by the incident light to generate a narrow resonant line shape (regarded as a discrete state). The coupling of the two resonances generates the double Fano formant of the narrow line shape. The resonance wavelengths are 938.0 nm and 1365.6 nm, respectively. Four media with RIs of 1.31, 1.33, 1.35, and 1.37 were used to replace the water in the cavity. The S of the two peaks of the sensor were 693.9 nm/RIU and 985.6 nm/RIU, and FWHMs were 5.8 nm and 8.3 nm, respectively. FOMs were 119.7 and 119.0, respectively. In addition, by changing the polarization of incident light, the measured resonant wavelength is invariant and insensitive to polarization. The near-field enhancement of the MA can not only be limited to the medium between the antenna and the metal mirror layer, but also can expose the near-field enhancement of MA to RI in the external environment to increase the S of the MA to RI. Jung *et al.* proposed an infrared MA with a nanogap as the RI sensor[189]. The etched MA was measured in air ($n = 1$) and oil ($n = 1.296$), where the maximum value of FOM* was about 273, and the S was 1091 nm/RIU. The nanocracking MA has great potential as a high-performance plasmonic biosensor.

Graphene has attracted more and more attention in recent years due to its excellent electrical, mechanical, and chemical properties. In optical sensors, absorbers with ultra-narrow bandwidth have broad application prospects. Yan *et al.* proposed an ultra-narrow-band PA by coating graphene-dielectric-metal with a dielectric grating. The structure of the absorber is shown in Figs. 10(a) and 10(b). The ultra-narrow band is generated by the light dissipation of graphene and the GMR of the dielectric grating. When the RI increases from 1.00 to 1.04, the relationship between the resonant wavelength and RI is shown in Figs. 10(c) and 10(d). High performance of sensing with $S = 150$ nm/RIU, FOM = 50, FOM* = 25,374 around the resonance wavelength is achieved[190]. Shortly thereafter, Yan *et al.* again proposed a graphene-dielectric-metal-dielectric-metal structure[191], in which lattice plasmon resonance is generated by collective resonance mediated by diffraction coupling of the wide LSPRs mode of metal nanoparticles and the narrow diffraction mode of the array. The structure achieves a high optical S of 288 nm/RIU and an optimal RI sensing value (FOM) of up to 72, providing practical applications in biomedical sensors.

3.3. Switches

Optical switching is a kind of process in which a certain parameter of light (intensity, wavelength, polarization, etc.) is changed from one state to another state rapidly, reversibly, and discontinuously under a certain drive[192–194]. As the basic component of an optical network, the optical switch plays an important role in optical communication technology. In recent years, many studies have shown that MPAs can be used as a light switch. The researchers propose an intensity switch based on a graphene plasmonic PA[195], which consists of a perfectly conductive layer as a substrate, a flexible poly(dimethyl siloxane) film as an intermediate buffer layer, and an array of graphene disks with nanoslits as a top. The simulation results show that the structure has three absorption peaks reaching 99.5% or more. Due to the destruction of symmetry of the graphene disk, the structure is sensitive to polarization. So, the reflection intensity matches perfectly with the ideal Marius law. This property represents its potential application in optical switches. The graphene resonance wavelength and the Fermi energy show a nearly perfect linear relationship when voltage is applied to the graphene structure to change the Fermi energy. The researchers realized an

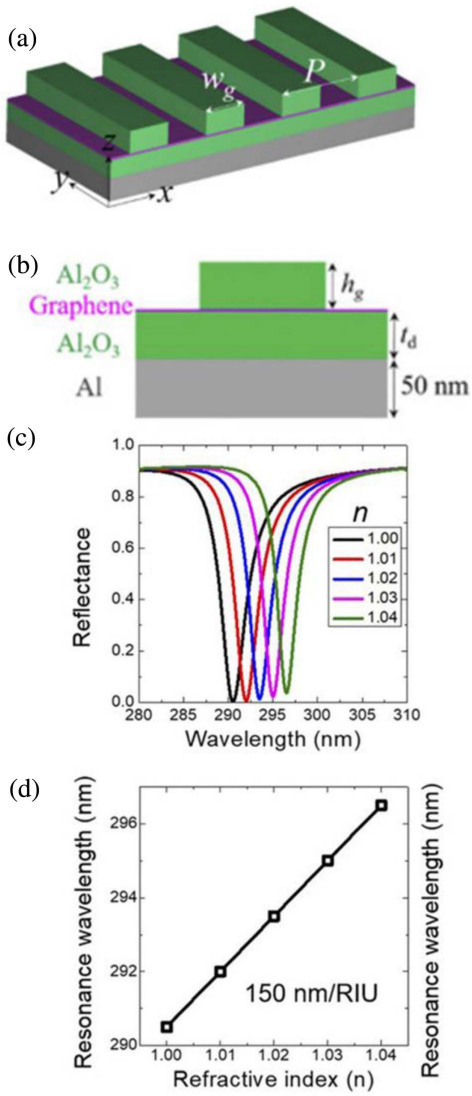

Fig. 10. (a) Schematic 3D view of the proposed graphene structure. (b) The front view of a unit cell of the structure. (c) Reflection spectra of the graphene structure in different environment media. (d) The corresponding S[190].

electro-optical switch by taking a Fermi energy of 0.8 eV (reflection approaching zero) to the off state and a Fermi energy of 0.85 eV (reflection approaching 0.8) to the on state. Two years later, Liu *et al.* placed a continuous graphene monolayer on the top of a metal substrate with an oblique-slit air cavity array to structure a plasmonic graphene absorber (PGA)[196]. This PGA has three main absorption peaks with the intensity close to 100%, and the Q factor of absorption peaks can reach up to 190. Absorbers that have high-Q factors can effectively improve the efficiency of the artificial manipulation for the switch and modulator. Moreover, when the Fermi energy of this PGA changed from 1.17 eV to 1.20 eV, the intensity of this PGA sharply increased 82%. All properties suggest the potential of this absorber as an efficient switch. Since graphene is a two-dimensional material, some researchers regarded graphene as a zero-thickness impedance sheet and obtained the graphene with different impedances by changing the chemical potential of graphene[197]. The graphene sheets of different sizes were regularly arranged on the uppermost layer of the absorber to fabricate an FP cavity. Based on the impedance matching principle and the reflection interference theory, this graphene PA achieved spectral absorption up to 90% in a broadband range. In this way, a switch whose intensity modulation depth exceeded 83% was realized in a wideband range [Fig. 11(a)]. Since the existing chip technologies are based on monocrystalline silicon, silicon photonics becomes the most promising direction of photonic integrated circuits in the future due to its low loss of optical transmission, high integration, and CMOS platform compatibility[198]. The metallic absorber can realize effective narrow-band absorption and realize photothermal conversion on the nanometer scale[199]. Based on this principle, it can be used to realize all-optical control based on the photothermal effect. Due to the compact structure of PAs, they can be directly integrated on silicon components, ensuring efficient heat transfer and shorter response time[200]. This use of light to control the photothermal effect opens new ways for optical switches.

In addition, the manufacturing process of the DTA is compatible with CMOS technology. DTA-based optical switches are also an important development direction. In recent years, VO_2 has attracted much attention due to its low phase transition temperature ($T = 68$°C), high speed (picosecond), and excellent thermal stability. In Section 2.4, we introduced a DTA [Fig. 7(g)] based on VO_2[141]. The VO_2 phase can be controlled by changing the temperature, and the absorption and wavelength relationship diagram of the metal phase and insulator phase can be obtained through simulation. At the wavelength $\lambda = 780$ nm, researchers defined VO_2 of the insulator phase as the "open" state and VO_2 of the metal phase as the "off" state [Fig. 11(b)]. So, a DTA-based optical switch is realized by using the phase transition of VO_2. Similarly, Yu *et al.* utilized a tunable absorber with VO_2-assisted metasurface to achieve features of switches in the infrared band[201]. This MPA has two near-unity absorption peaks ($\lambda_1 = 3049.9$ nm, $\lambda_2 = 3173.6$ nm) with the Q-factor of 1112.8 and 1381.1, respectively. At 60°C, VO_2 is in the dielectric phase, and the absorption of λ_1 and λ_2 is 97.74% and 99.95%. At 88°C, VO_2 is in the metallic phase, and the absorption of λ_1 and λ_2 is 8.37% and 19.16%, respectively. The modulation depths are up to 16.1 dB at λ_1 and 31.8 dB at λ_2 [Fig. 11(c)]. It is almost the largest reflection modulation depth currently available[202]. Moreover, the phase related switching of VO_2 can also be excited by ultrafast lasers with switching time in the picosecond range. Otherwise, nonlinear materials such as lithium niobate ($LiNbO_3$) crystals[203–206] and electro-optic effective materials lithium tantalite ($LiTaO_3$)[207–209] also have the capability for applications in electrical or optical switching via the plasmonic light absorber platform.

3.4. Structural colors

Colors play a most indispensable role in our visual world. In daily life, the colors we often use mainly come from various pigments. Unlike everyday pigments, the large backs of many beetles and the wings of butterflies can also show various colors in

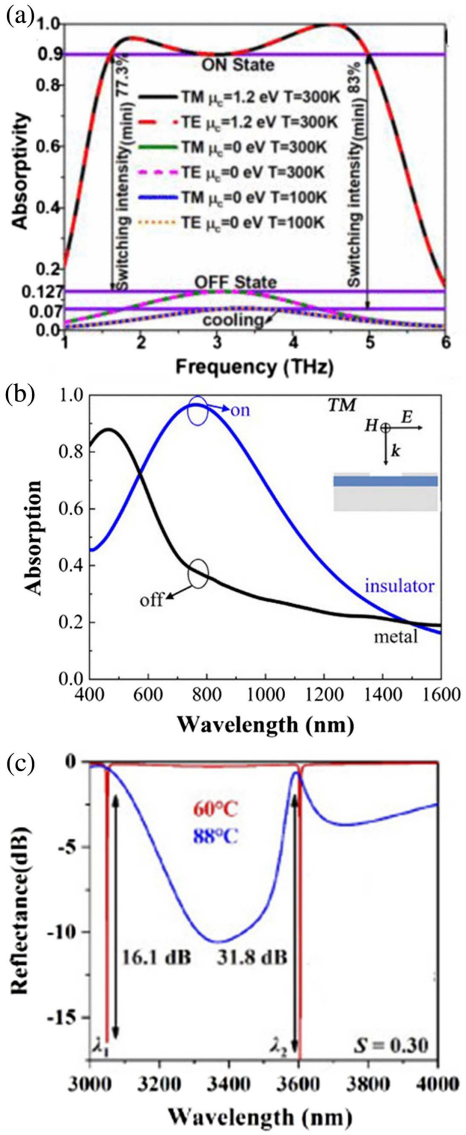

Fig. 11. (a) Absorption spectra for different graphene chemical potentials and temperatures. Schematic of ON and OFF states[197]. (b) Illustration of the switchable state[141]. (c) The reflection spectra of the designed metasurface at 60°C (insulator phase) and 88°C (metallic phase)[201].

nature. The main causes of this phenomenon are interference and diffraction of light. We call these structural colors that can be produced by artificially controlling structural morphology and geometry. The generation of structural colors by MPA is realized because the researchers reasonably designed the MPA, and the wavelength of the reflected wave is manually controlled in the visible band.

MPA-based structural colors have a wide range of applications in anti-counterfeiting[26,27], high-resolution printing[210], optical data archiving[211], color filters[212,213], and color displays based on nanophotonic structures[214,215]. Therefore, MPA-based structural color generation has been investigated by researchers, and FP resonance, LSPR, and Mie resonance are widely used in structural colors generation. The common FP resonance achieves the absorption and reflection of a specific wavelength band through destructive and constructive interference caused by the phase shift generated by the incident wave propagating in the lossless medium of the FP resonator. Park and Lee[216] utilized deposition processes to prepare MPA with Pt, Ti, and Al triple-layer structures on rigid and flexible

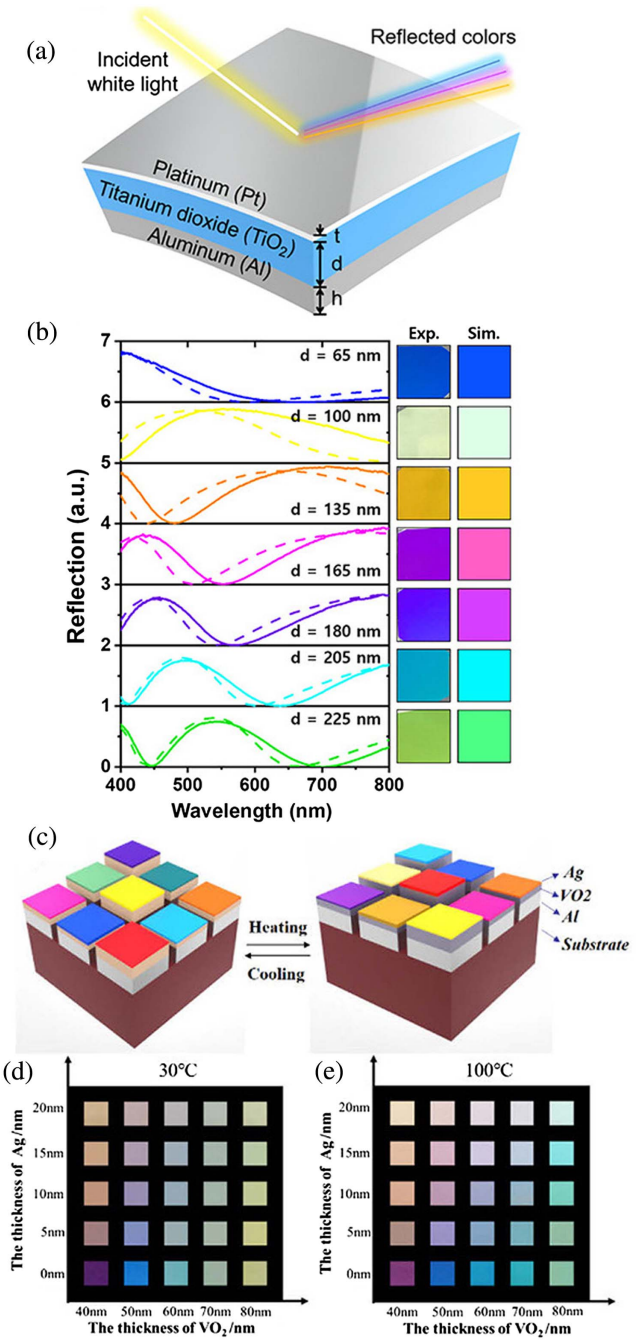

Fig. 12. (a) Illustration of asymmetric FP nanocavity absorber. Reproduced with permission from Ref. [216] Copyright 2021, American Chemical Society. (b) Measured (solid line) and simulated (dashed line) reflectance spectra and corresponding colors at different FP cavity thicknesses[216]. (c) Illustration of the proposed VO_2 dynamic structural colors. The reflected light varies with Ag film and VO_2 thickness at (d) 30°C and (e) 100°C[217].

substrates [Fig. 12(a)]. The near-perfect absorption of Pt promotes reflection suppression in the resonant band of visible light, while producing good reflection in the non-resonant band. Bright and vivid colors can be achieved with a reflection efficiency of up to 87.5% over the entire visible wavelength range. But, the absorber can only display different colors by adjusting the thickness of the dielectric layer [Fig. 12(b)]. In the front, a tunable MPA was constructed by phase-change material and realized the transformation of phase-change materials by changing the external environment. The optical path difference of the coherent light can be changed, due to utilizing VO_2 as the FP cavity material, where the change of the RI of the resonator cavity is controlled by changing the temperature. Based on this principle, dynamic structural colors can be realized. Zhao *et al.* utilized VO_2 as the material of the resonant cavity, and the Ag layer and the Al layer were used as the top and bottom of the FP cavity, respectively [Fig. 12(c)] to construct a dynamic structural color generating device[217]. When the temperature changes, the structural color can be dynamically switched [Figs. 12(d) and 12(e)]. However, VO_2 is stable in its phases only within a certain temperature range. In contrast, the primary phases of $Ge_2Sb_2Te_5$ (GST), both amorphous and crystalline, are stable in most applications[211]. A symmetric MA structure to generate a wide gamut was achieved by Rui and co-workers via a theoretical design structure with a metal nanodisk array, a dielectric buffer layer, a GST thin film, and a metal mirror[218]. The absorber exhibits dynamic color properties by changing the phase of the PCM. Furthermore, the hue and saturation of the structural colors can be tuned by tuning the structural geometry of the nanodisks, due to the interaction of localized/propagating surface plasmons, FP cavity modes, and Wood anomalies at different resonance frequencies. Structural colors cost more than traditional pigments, but offer higher tunability, durability, and chemical resistance. Therefore, structural colors show extremely high application value in some special applications and harsh environments. The advantages and disadvantages of opto-electronic devices based on MPA are illustrated in Table 2.

4. Conclusions and Future Outlook

In this review, we summarized some of the research developments and applications of PAs in the past few years. In the past two years, the emergence of new concepts and new methods has led to the rapid development of PAs and has shown great potential in application. Great attention has been attracted since MPAs were proposed in 2008. The latest developments of PAs with single-band, dual-band, multi-band, wide-band, narrow-band, and tunable light absorption have been summarized to show their unique characteristics and applications. The shortcomings of the related PAs and the latest improvements were introduced as well. Moreover, we further introduced the application of perfect absorption in solar cells, sensor switches, and structural colors. We also presented the main challenges and prospects in these fields. We believe that novel PAs for wide applications in opto-electronic fields will continuously progress with breakthrough advances in future technology and science.

However, in actual industrial production, we must consider the significant factors for all absorbers. First of all, in most absorbers, noble metals, such as gold and Ag, are often used as substrates or resonators. For some large-scale optical devices, due to the high ohmic loss and heat generation, the aim of cost-control, and the intrinsic characteristic of scarce resources, using noble metals as the substrate will extremely hamper the wide applications. That is, the new resonant materials should be considered for the plasmonic or plasmon-like materials, such as the high-index dielectrics and doped semiconductors. Secondly, complex patterned antenna layers are widely designed and used in the absorbers, even with a need of size down to the nanometer scale. Therefore, multi-step and high-cost lithography methods such as FIB, electron beam lithography (EBL), and reactive ion etching (RIE) are used as typical methods. The high cost and low yield of these technologies will limit the application of PAs. In addition, the solar absorber needs to be insensitive to polarization and incident angle and also requires high stability for the temperature and chemical surroundings. In the development of optical switches, not only temperature-controlled optical switches and electronically controlled optical switches, but also light-controlled all-optical switches, all have the need for the realization of the concept of higher-speed switch response and high signal-to-noise ratio. To sum up, a lot of great efforts have been made for the development of the PAs in these years, leading to the emergence of a series of new science and technologies for applications in opto-electronic devices. With the rapid development, we have reason to believe that the PA has a bright future.

Table 2. The Advantages and Disadvantages of Opto-Electronic Devices Based on MPA.

Opto-Electronic Devices	Advantage	Disadvantage	Reference
Solar cell	High efficiency	Expensiveness	[67,145–148]
Sensor	Sensitivity	Complex structure	[185,189–191]
Switch	Integration; high switching ratio	High preparation requirements	[140,141,197,201]
Structural color	Stability; environmental protection	High cost; low production efficiency	[210,216,217]

Acknowledgement

This work was supported by the National Natural Science Foundation of China (Nos. 51761015, 11764020, 11804134, and 62065007) and Natural Science Foundation of Jiangxi Province (Nos. 20182BCB22002, 20202BBEL53036, and 20202BAB201009).

†These authors contributed to this work equally.

References

1. J. X. Li, S. W. Yang, C. H. Wang, W. T. Joines, and Q. H. Liu, "Metamaterial cavity for the isolation enhancement of closely positioned dual-polarized relay antenna arrays," Microw. Opt. Techn. Lett. **59**, 857 (2017).
2. S. K. Patel, K. H. Shah, and Y. P. Kosta, "Multilayer liquid metamaterial radome design for performance enhancement of microstrip patch antenna," Microw. Opt. Techn. Lett. **60**, 600 (2018).
3. C. M. Saleh, D. Bensafieddine, E. M. Laamari, and M. Bouzouad, "A zero-index metamaterial single layer superstrate for patch antenna gain enhancement," Acta Phys. Pol. **128**, B307 (2015).
4. C. P. Scarborough, Z. H. Jiang, D. H. Werner, C. Rivero-Baleine, and C. Drake, "Experimental demonstration of an isotropic metamaterial super lens with negative unity permeability at 8.5 MHz," Appl. Phys. Lett. **101**, 014101 (2012).
5. Y. H. Zhao, A. A. Nawaz, S. C. S. Lin, Q. Z. Hao, B. Kiraly, and T. J. Huang, "Nanoscale super-resolution imaging via a metal–dielectric metamaterial lens system," J. Phys. D **44**, 415101 (2011).
6. X. J. Huang, H. L. Yang, Z. Y. Shen, J. Chen, H. I. Lin, and Z. T. Yu, "Water-injected all-dielectric ultra-wideband and prominent oblique incidence metamaterial absorber in microwave regime," J. Phys. D **50**, 385304 (2017).
7. C. L. Xu, B. K. Wang, M. B. Yan, Y. Q. Pang, W. J. Wang, Y. Y. Meng, J. F. Wang, and S. B. Qu, "An optical-transparent metamaterial for high-efficiency microwave absorption and low infrared emission," J. Phys. D **53**, 135109 (2019).
8. N. Landy, S. Sajuyigbe, J. Mock, D. Smith, and W. Padilla, "Perfect metamaterial absorber," Phys. Rev. Lett. **100**, 207402 (2008).
9. J. Bucinskas, L. Nickelson, and V. Shugurovas, "Microwave scattering and absorption by a multilayered lossy metamaterial-glass cylinder," Prog. Electromagn. Res. **105**, 103 (2010).
10. W. Luo, X. Wang, S. Wang, X. Wang, Z. Liu, L. Li, F. Hu, Y. Wen, and J. Zhou, "Miniaturization of dielectric ceramic-based metamaterial perfect absorber," Appl. Phys. Lett. **120**, 013502 (2022).
11. J. Y. Jung, J. Lee, D. G. Choi, J. H. Choi, J. H. Jeong, E. S. Lee, and D. P. Neikirk, "Wavelength-selective infrared metasurface absorber for multispectral thermal detection," IEEE Photonics J. **7**, 6804210 (2015).
12. S. W. Dai, D. Zhao, Q. Li, and M. Qiu, "Double-sided polarization-independent plasmonic absorber at near-infrared region," Opt. Express **21**, 13125 (2013).
13. D. Wu, R. F. Li, Y. M. Liu, Z. Y. Yu, L. Yu, L. Chen, C. Liu, R. Ma, and H. Ye, "Ultra-narrow band perfect absorber and its application as plasmonic sensor in the visible region," Nanoscale Res. Lett. **12**, 427 (2017).
14. M. L. Li, B. Muneer, Z. X. Yi, and Q. Zhu, "A broadband compatible multi-spectral metamaterial absorber for visible, near-infrared, and microwave bands," Adv. Opt. Mater. **6**, 1701238 (2018).
15. B. Grzeskiewicz, A. Sierakowski, J. Marczewski, N. Palka, and E. Wolarz, "Polarization-insensitive metamaterial absorber of selective response in terahertz frequency range," J. Opt. **16**, 105104 (2014).
16. H. Kong, G. F. Li, Z. M. Jin, G. H. Ma, Z. W. Zhang, and C. L. Zhang, "Polarization-independent metamaterial absorber for terahertz frequency," J. Infrared Millim. Terahertz Waves **33**, 649 (2012).
17. X. Liu, T. Tyler, T. Starr, A. F. Starr, N. M. Jokerst, and W. J. Padilla, "Taming the blackbody with infrared metamaterials as selective thermal emitters," Phys. Rev. Lett. **107**, 045901 (2011).
18. M. L. Hakim, T. Alam, A. F. Almutairi, M. F. Mansor, and M. T. Islam, "Polarization insensitivity characterization of dual-band perfect metamaterial absorber for K band sensing applications," Sci. Rep. **11**, 17829 (2021).
19. J. Luo, H. Chu, R. Peng, M. Wang, J. Li, and Y. Lai, "Ultra-broadband reflectionless Brewster absorber protected by reciprocity," Light Sci. Appl. **10**, 89 (2021).
20. F. Wu, X. H. Wu, S. Y. Xiao, G. H. Liu, and H. J. Li, "Broadband wide-angle multilayer absorber based on a broadband omnidirectional optical Tamm state," Opt. Express **29**, 23976 (2021).
21. J. Luo, H. Chu, R. Peng, M. Wang, J. Li, and Y. Lai, "Ultra-broadband reflectionless Brewster absorber protected by reciprocity," Light Sci. Appl. **10**, 89 (2021).
22. Y. Zhou, Z. Qin, Z. Liang, D. Meng, H. Xu, D. R. Smith, and Y. Liu, "Ultra-broadband metamaterial absorbers from long to very long infrared regime," Light Sci. Appl. **10**, 138 (2021).
23. C. M. Watts, X. Liu, and W. J. Padilla, "Metamaterial electromagnetic wave absorbers," Adv. Mater. **24**, 98 (2012).
24. D. Yevick and D. J. Thomson, "Impedance-matched absorbers for finite-difference parabolic equation algorithms," J. Acoust. Soc. Am. **107**, 1226 (2000).
25. N. Luhmann, D. Hoj, M. Piller, H. Kähler, M.-H. Chien, R. G. West, U. L. Andersen, and S. Schmid, "Ultrathin 2 nm gold as impedance-matched absorber for infrared light," Nat. Commun. **11**, 2161 (2020).
26. M. Y. Pan, L. B. Wang, S. L. Dou, J. P. Zhao, H. B. Xu, B. Wang, L. P. Zhang, X. B. Li, L. Pan, and Y. Li, "Recent advances in colloidal photonic crystal-based anti-counterfeiting materials," Crystals **9**, 417 (2019).
27. C. Jung, Y. Yang, J. Jang, T. Badloe, T. Lee, J. Mun, S. W. Moon, and J. J. Rho, "Near-zero reflection of all-dielectric structural coloration enabling polarization-sensitive optical encryption with enhanced switchability," Nanophotonics **10**, 919 (2021).
28. G. H. Rui, C. C. Ding, B. Gu, Q. Q. Gan, Q. W. Zhan, and Y. P. Cui, "Symmetric $Ge_2Sb_2Te_5$ based metamaterial absorber induced dynamic wide-gamut structural color," J. Opt. **22**, 085003 (2020).
29. S. U. Kim, S. H. Lee, and I. H. Lee, "Generation of intensity-tunable structural color from helical photonic crystals for full color reflective-type display," Sci. Adv. **4**, 8829 (2018).
30. S. L. Li, M. C. Panmai, S. L. Tie, Y. Xu, J. Xiang, and S. Lan, "Regulating disordered plasmonic nanoparticles into polarization sensitive metasurfaces," Nanophotonics **10**, 1553 (2021).
31. H. Z. Zhu, Q. Li, C. N. Tao, Y. Hong, Z. Q. Xu, W. D. Shen, S. Kaur, P. Ghosh, and M. Qiu, "Multispectral camouflage for infrared, visible, lasers and microwave with radiative cooling," Nat. Commun. **12**, 1805 (2021).
32. D. J. Ironside, R. Salas, P. Y. Chen, K. Q. Le, A. Alu, and S. R. Bank, "Enhancing THz generation in photomixers using a metamaterial approach," Opt. Express **27**, 9481 (2019).
33. R. M. Saadabad, L. Huang, and A. E. Miroshnichenko, "Polarization-independent perfect absorber enabled by quasibound states in the continuum," Phys. Rev. B **104**, 235405 (2021).
34. J. F. Zhang, Q. L. Hong, J. L. Zou, Q. Meng, S. Q. Qin, and Z. H. Zhu, "Ultra-narrowband visible light absorption in a monolayer MoS_2 based resonant nanostructure," Opt. Express **28**, 27608 (2020).
35. Z. B. Li, X. A. Sun, C. R. Ma, J. Li, X. P. Li, B. O. Guan, and K. Chen, "Ultra-narrow-band metamaterial perfect absorber based on surface lattice resonance in a WS_2 nanodisk array," Opt. Express **29**, 27084 (2021).
36. J. Xiang, M. Panmai, S. W. Bai, Y. H. Ren, G. C. Li, S. L. Li, J. Liu, J. T. Li, M. X. Zeng, J. C. She, Y. Xu, and S. Lan, "Crystalline silicon white light sources driven by optical resonances," Nano Lett. **21**, 2397 (2021).
37. Y. T. Chen, J. Dai, M. Yan, and M. Qiu, "Metal-insulator-metal plasmonic absorbers: influence of lattice," Opt. Express **22**, 30807 (2014).
38. B. Gerislioglu, L. Dong, A. Ahmadivand, H. Hu, P. Nordlander, and N. J. Halas, "Monolithic metal dimer-on-film structure: new plasmonic properties introduced by the underlying metal," Nano Lett. **20**, 2087 (2020).
39. M. Pan, Z. C. Su, Z. F. Yu, P. H. Wu, H. G. Jile, Z. Yi, and Z. Q. Chen, "A narrowband perfect absorber with high Q-factor and its application in sensing in the visible region," Results Phys. **19**, 103415 (2020).
40. D. Hu, T. H. Meng, H. Y. Wang, Y. K. Ma, and Q. F. Zhu, "Ultra-narrowband terahertz perfect metamaterial absorber for refractive index sensing application," Results Phys. **19**, 103567 (2020).
41. A. Vazquez-Guardado, M. Money, N. Mckinney, and D. Chanda, "Multispectral infrared spectroscopy for robust plastic identification," Appl. Opt. **54**, 7396 (2015).

42. X. L. Wu, Y. Zheng, Y. Luo, J. G. Zhang, Z. Yi, X. W. Wu, S. B. Cheng, W. X. Yang, Y. Yu, and P. H. Wu, "A four-band and polarization-independent BDS-based tunable absorber with high refractive index sensitivity," Phys. Chem. Chem. Phys. **23**, 26864 (2021).
43. W. H. Yang, S. M. Xiao, Q. H. Song, Y. L. Liu, Y. K. Wu, S. Wang, J. Yu, J. C. Han, and D. P. Tsai, "All-dielectric metasurface for high-performance structural color," Nat. Commun. **11**, 1864 (2020).
44. Q. B. Fan, M. Z. Liu, C. Zhang, W. Q. Zhu, Y. L. Wang, P. C. Lin, F. Yan, L. Chen, H. J. Lezec, Y. Q. Lu, A. Agrawal, and T. Xu, "Independent amplitude control of arbitrary orthogonal states of polarization via dielectric metasurfaces," Phys. Rev. Lett. **125**, 267402 (2020).
45. F. Yan, Q. Li, H. Tian, Z. W. Wang, and L. Li, "An ultrahigh *Q*-factor dual-band terahertz perfect absorber with a dielectric grating slit waveguide for sensing," J. Phys. D **53**, 235103 (2020).
46. Y. H. Ko, N. Razmjooei, H. Hemmati, and R. Magnusson, "Perfectly-reflecting guided-mode-resonant photonic lattices possessing Mie modal memory," Opt. Express **29**, 26971 (2021).
47. N. Razmjooei, Y. H. Ko, F. A. Simlan, and R. Magnusson, "Resonant reflection by microsphere arrays with AR-quenched Mie scattering," Opt. Express **29**, 19183 (2021).
48. G. C. Li, J. Xiang, Y. L. Zhang, F. Deng, M. Panmai, W. J. Zhuang, S. Lan, and D. Y. Lei, "Mapping the magnetic field intensity of light with the nonlinear optical emission of a silicon nanoparticle," Nano Lett. **21**, 2453 (2021).
49. H. Lin, B. C. P. Sturmberg, K.-T. Lin, Y. Yang, X. Zheng, T. K. Chong, C. M. Sterke, and B. Jia, "A 90-nm-thick graphene metamaterial for strong and extremely broadband absorption of unpolarized light," Nat. Photonics **13**, 270 (2019).
50. S. Lee, J. Song, and S. Kim, "Graphene perfect absorber with loss adaptive *Q*-factor control function enabled by quasi-bound states in the continuum," Sci. Rep. **11**, 22819 (2021).
51. X. K. He, Z. Y. Sun, Q. T. Zou, L. Y. Wu, and J. B. Jiang, "Electrochemical behavior of Co (II) reduction for preparing nanocrystalline Co catalyst for hydrogen evolution reaction from 1-ethyl-3-methylimidazolium bisulfate and ethylene glycol system," J. Electrochem. Soc. **166**, D57 (2019).
52. M. L. Shi, F. Lan, P. Mazumder, M. Aghadjani, Z. Q. Yang, L. Meng, and J. Zhou, "Enhanced quadruple-resonant terahertz metamaterial with asymmetric hybrid resonators," Opt. Mater. **75**, 533 (2018).
53. H. Li, J. Niu, and G. Wang, "Dual-band, polarization-insensitive metamaterial perfect absorber based on monolayer graphene in the mid-infrared range," Results Phys. **13**, 102313 (2019).
54. Z. Q. Liu, G. Q. Liu, G. L. Fu, X. S. Liu, and Y. Wang, "Multi-band light perfect absorption by a metal layer-coupled dielectric metamaterial," Opt. Express **24**, 5020 (2016).
55. Y. Y. Wang, Z. Q. Chen, D. Y. Xu, Z. Yi, X. F. Chen, J. Chen, Y. J. Tang, P. H. Wu, G. F. Li, and Y. G. Yi, "Triple-band perfect metamaterial absorber with good operating angle polarization tolerance based on split ring arrays," Results Phys. **16**, 102951 (2020).
56. Q. Li, J. Lu, P. Gupta, and M. Qiu, "Engineering optical absorption in graphene and other 2D materials: advances and applications," Adv. Opt. Mater. **7**, 1900595 (2019).
57. H. J. Li, B. Chen, X. Zhai, L. Xu, and L. L. Wang, "Tunable ultra-multispectral metamaterial perfect absorbers based on out-of-plane metal-insulator-graphene heterostructures," J. Lightwave Technol. **38**, 1858 (2019).
58. L. Zhou, Y. Tan, D. Ji, B. Zhu, P. Zhang, J. Xu, Q. Gan, Z. Yu, and J. Zhu, "Self-assembly of highly efficient, broadband plasmonic absorbers for solar steam generation," Sci. Adv. **2**, e1501227 (2016).
59. L. Zhou, Y. Tan, and J. Zhu, "Broadband plasmonic absorbers for highly efficient solar steam generation," in *Optical Nanostructures and Advanced Materials for Photovoltaics* (2015), paper PW3B.3.
60. P. D. Dongare, A. Alabastri, O. Neumann, P. Nordlander, and N. J. Halas, "Solar thermal desalination as a nonlinear optical process," Proc. Natl. Acad. Sci. U.S.A. **116**, 13182 (2019).
61. K. T. Lin, H. Lin, T. S. Yang, and B. H. Jia, "Structured graphene metamaterial selective absorbers for high efficiency and omnidirectional solar thermal energy conversion," Nat. Commun. **11**, 1389 (2020).
62. Y. Liu, F. Wang, X. Wang, X. Wang, E. Flahaut, X. Liu, Y. Li, X. Wang, Y. Xu, and Y. Shi, "Planar carbon nanotube-graphene hybrid films for high-performance broadband photodetectors," Nat. Commun. **6**, 8589 (2015).
63. Y. Liu, Q. Hu, Y. Wang, Y. Xie, Z. Zhao, Z. Dong, J.-L. Zhu, W. Chu, N. Yang, J. Wei, W. Ma, and J.-L. Sun, "High-performance, ultra-broadband, ultraviolet to terahertz photodetectors based on suspended carbon nanotube films," ACS Appl. Mater. Interfaces **10**, 36304 (2018).
64. Y. L. Liao and Y. Zhao, "Ultra-narrowband dielectric metamaterial absorber with ultra-sparse nanowire grids for sensing applications," Sci. Rep. **10**, 3966 (2020).
65. H. J. Zhang, Z. Q. Liu, H. Z. Zhong, G. Q. Liu, X. S. Liu, and J. Q. Wang, "Metal-free plasmonic refractory core-shell nanowires for tunable all-dielectric broadband perfect absorbers," Opt. Express **28**, 37049 (2020).
66. S. Ijaz, A. Rana, Z. Ahmad, B. Rehman, M. Zubair, and M. Mehmood, "Exploiting zirconium nitride for an efficient heat-resistant absorber and emitter pair for solar thermophotovoltaic systems," Opt. Express **29**, 31537 (2021).
67. Y. Li, Z. Liu, P. Pan, X. Liu, G. Fu, Z. Liu, H. Luo, and G. Liu, "Semiconductor-nanoantenna-assisted solar absorber for ultra-broadband light trapping," Nanoscale Res. Lett. **15**, 816 (2020).
68. K. L. Zhang, J. Y. Zhang, Z. L. Hou, S. Bi, and Q. L. Zhao, "Multifunctional broadband microwave absorption of flexible graphene composites," Carbon **141**, 608 (2019).
69. J. Liu, W. Ma, W. Chen, G. Yu, Y. Chen, X. Deng, and C. Yang, "Numerical analysis of an ultra-wideband metamaterial absorber with high absorptivity from visible light to near-infrared," Opt. Express **28**, 23748 (2020).
70. Y. Jin and K. Yu, "Broadband single-channel coherent perfect absorption with a perfect magnetic mirror," Opt. Express **28**, 35108 (2020).
71. L. Zhao, H. Liu, Z. H. He, and S. K. Dong, "All-metal frequency-selective absorber/emitter for laser stealth and infrared stealth," Appl. Opt. **57**, 1757 (2018).
72. Y. J. Cai, K. D. Xu, N. Feng, R. Guo, H. Lin, and J. Zhu, "Anisotropic infrared plasmonic broadband absorber based on graphene-black phosphorus multilayers," Opt. Express **27**, 3101 (2019).
73. H. Ullah, A. D. Khan, M. Noman, and A. U. Rehman, "Novel multi-broadband plasmonic absorber based on a metal-dielectric-metal square ring array," Plasmonics **13**, 591 (2017).
74. X. Ruan, W. Dai, W. Wang, C. Ou, Q. Xu, Z. Zhou, Z. Wen, C. Liu, J. Hao, Z. Guan, and H. Xu, "Ultrathin, broadband, omnidirectional, and polarization-independent infrared absorber using all-dielectric refractory materials," Nanophotonics **10**, 1683 (2021).
75. Y. Zhou, Z. Qin, Z. Liang, D. Meng, H. Xu, D. R. Smith, and Y. Liu, "Ultra-broadband metamaterial absorbers from long to very long infrared regime," Light Sci. Appl. **10**, 138 (2021).
76. Z. Qin, X. Shi, F. Yang, E. Hou, D. Meng, C. Sun, R. Dai, S. Zhang, H. Liu, H. Xu, and Z. Liang, "Multi-mode plasmonic resonance broadband LWIR metamaterial absorber based on lossy metal ring," Opt. Express **30**, 473 (2022).
77. S. Yue, M. Hou, R. Wang, H. Guo, Y. Hou, M. Li, Z. Zhang, Y. Wang, and Z. Zhang, "Ultra-broadband metamaterial absorber from ultraviolet to long-wave infrared based on CMOS-compatible materials," Opt. Express **28**, 31844 (2020).
78. T. Liu and J. Takahara, "Ultrabroadband absorber based on single-sized embedded metal-dielectric-metal structures and application of radiative cooling," Opt. Express **25**, A612 (2017).
79. A. Hoque, M. T. Islam, A. F. Almutairi, and M. Faruque, "Design of split hexagonal patch array shaped nano-metaabsorber with ultra-wideband absorption for visible and UV spectrum application," Nanoscale Res. Lett. **14**, 393 (2019).
80. Q. Cheng, P. Li, J. Lu, X. Yu, and H. L. Zhou, "Silicon complex grating with different groove depths as an absorber for solar cells," J. Quant. Spectrosc. Radiat. Transfer **132**, 70 (2014).
81. P. Bouchon, C. Koechlin, F. Pardo, R. Haïdar, and J. L. Pelouard, "Wideband omnidirectional infrared absorber with a patchwork of plasmonic nanoantennas," Opt. Lett. **37**, 1038 (2012).
82. N. Nguyen-Huu, J. Pistora, and M. Cada, "Dual broadband infrared absorptance enhanced by magnetic polaritons using graphene-covered compound metal grating," Opt. Express **27**, 30182 (2019).
83. J. L. Song, M. T. Si, Q. Cheng, and Z. X. Luo, "Two-dimensional trilayer grating with a metal/insulator/metal structure as a thermophotovoltaic emitter," Appl. Opt. **55**, 1284 (2016).
84. A. P. Raman, M. A. Anoma, L. Zhu, E. Rephaeli, and S. Fan, "Passive radiative cooling below ambient air temperature under direct sunlight," Nature **515**, 540 (2014).

85. S. Kamau, S. Hassan, K. Alnasser, H. L. Zhang, J. B. Cui, and Y. K. Lin, "Broadband absorption in patterned metal/weakly-absorbing-spacer/metal with graded photonic super-crystal," Photonics **8**, 114 (2021).
86. E. Rephaeli, A. Raman, and S. Fan, "Ultrabroadband photonic structures to achieve high-performance daytime radiative cooling," Nano Lett. **13**, 1457 (2013).
87. A. Saib, L. Bednarz, R. Daussin, C. Bailly, X. Lou, J.-M. Thomassin, C. Pagnoulle, C. Detrembleur, R. Jerome, and I. Huynen, "Carbon nanotube composites for broadband microwave absorbing materials," IEEE Trans. Microwave Theory Tech. **54**, 2745 (2006).
88. D. Katzen, E. Levy, and Y. Mastai, "Thin films of silica–carbon nanocomposites for selective solar absorbers," Appl. Surf. Sci. **248**, 514 (2005).
89. M. K. Hedayati, M. Javaherirahim, B. Mozooni, R. Abdelaziz, A. Tavassolizadeh, V. S. K. Chakravadhanula, V. Zaporojtchenko, T. Strunkus, F. Faupel, and M. Elbahri, "Design of a perfect black absorber at visible frequencies using plasmonic metamaterials," Adv. Mater. **23**, 5410 (2011).
90. X. F. Chen, Y. Zhou, H. W. Han, X. Y. Wang, L. Zhou, Z. Yi, Z. J. Fu, X. W. Wu, G. F. Li, and L. C. Zeng, "Optical and magnetic properties of small-size core–shell Fe_3O_4@C nanoparticles," Mater. Today Chem. **22**, 100556 (2021).
91. L. Zhou, Y. Zhou, Y. F. Zhu, X. X. Dong, B. L. Gao, Y. Z. Wang, and S. Shen, "Broadband bidirectional visible light absorber with wide angular tolerance," J. Mater. Chem. C **4**, 391 (2016).
92. H. Lin, B. C. Sturmberg, K.-T. Lin, Y. Yang, X. Zheng, T. K. Chong, C. M. de Sterke, and B. Jia, "A 90-nm-thick graphene metamaterial for strong and extremely broadband absorption of unpolarized light," Nat. Photonics **13**, 270 (2019).
93. S. Thongrattanasiri, F. H. Koppens, and F. J. G. De Abajo, "Complete optical absorption in periodically patterned graphene," Phys. Rev. Lett. **108**, 047401 (2012).
94. F. Q. Zhou, F. Qin, Z. Yi, W. T. Yao, Z. M. Liu, X. W. Wu, and P. H. Wu, "Ultra-wideband and wide-angle perfect solar energy absorber based on Ti nanorings surface plasmon resonance," Phys. Chem. Chem. Phys. **23**, 17041 (2021).
95. T. Cao, K. Liu, L. Lu, H. C. Chui, and R. E. Simpson, "Large-area broadband near-perfect absorption from a thin chalcogenide film coupled to gold nanoparticles," ACS Appl. Mater. Interfaces **11**, 5176 (2019).
96. F. Kiani, F. Sterl, T. V. Tsoulos, K. Weber, H. Giessen, and G. Tagliabue, "Ultra-broadband and omnidirectional perfect absorber based on copper nanowire/carbon nanotube hierarchical structure," ACS Photonics **7**, 366 (2020).
97. F. Garcia-Vidal, J. Pitarke, and J. Pendry, "Effective medium theory of the optical properties of aligned carbon nanotubes," Phys. Rev. Lett. **78**, 4289 (1997).
98. L. Zhou, Y. Tan, J. Wang, W. Xu, Y. Yuan, W. Cai, S. Zhu, and J. Zhu, "3D self-assembly of aluminium nanoparticles for plasmon-enhanced solar desalination," Nat. Photonics **10**, 393 (2016).
99. W. Ali, M. F. Mideksa, K. Hou, H. D. Li, X. L. Wang, and Z. Y. Tang, "All-solution-processed ultrahigh broadband and wide-angle perfect absorber based on mxene-gold nanoparticles," Adv. Opt. Mater. **8**, 2000447 (2020).
100. C. C. Chang, S. C. Kuo, H. E. Cheng, H. T. Chen, and Z. P. Yang, "Broadband titanium nitride disordered metasurface absorbers," Opt. Express **29**, 42813 (2021).
101. Y. J. Jen, K. B. Yang, P. C. Lin, and M. H. Chung, "Deposited ultra-thin titanium nitride nanorod array as a plasmonic near-perfect light absorber," Sci. Rep. **10**, 22269 (2020).
102. W. Li, U. Guler, N. Kinsey, G. V. Naik, A. Boltasseva, J. Guan, V. M. Shalaev, and A. V. Kildishev, "Refractory plasmonics with titanium nitride: broadband metamaterial absorber," Adv. Mater. **26**, 7959 (2014).
103. D. H. Jiang, J. Qu, X. Xu, K. Liu, and W. J. Sun, "Light absorption characteristics of AAO/Ag NPs composite system," Acta Photonica Sin. **48**, 131001 (2019).
104. P. Bouchut, F. Geffraye, J. Bablet, and F. Emieux, "Ultrabroadband plasmonic induced transparency in random metamaterial with nanocavity," Opt. Mater. **98**, 109439 (2019).
105. N. Sharma, J. Bar-David, N. Mazurski, and U. Levy, "Metasurfaces for enhancing light absorption in thermoelectric photodetectors," ACS Photonics **7**, 2468 (2020).
106. H. Cai, Y. Sun, X. Wang, and S. Zhan, "Design of an ultra-broadband near-perfect bilayer grating metamaterial absorber based on genetic algorithm," Opt. Express **28**, 15347 (2020).
107. Y. Kim, P. Park, J. Jo, J. Lee, L. Jeong, J. Shin, J.-H. Lee, and H. J. Lee, "Ultrawideband electromagnetic metamaterial absorber utilizing coherent absorptions and surface plasmon polaritons based on double layer carbon metapatterns," Sci. Rep. **11**, 23045 (2021).
108. L. Chen, T. X. Ren, Y. Zhao, Q. Yu, Z. L. Huang, K. Zhang, J. Wen, F. Lin, and S. Q. Chen, "Polarization-independent wavefront manipulation of surface plasmons with plasmonic metasurfaces," Adv. Opt. Mater. **8**, 2000868 (2020).
109. Y. Cui, K. Fung, J. Xu, H. Ma, Y. Jin, S. He, and N. Fang, "Ultrabroadband light absorption by a sawtooth anisotropic metamaterial slab," Nano Lett. **12**, 1443 (2012).
110. S. He, F. Ding, L. Mo, and F. Bao, "Light absorber with an ultra-broad flat band based on multi-sized slow-wave hyperbolic metamaterial thin-films," Prog. Electromagn. Res. **147**, 69 (2014).
111. H. Deng, C. J. Mathai, S. Gangopadhyay, J. Gao, and X. Yang, "Ultra-broadband infrared absorption by tapered hyperbolic multilayer waveguides," Opt. Express **26**, 6360 (2018).
112. S. Hu, S. Yang, Z. Liu, B. Quan, J. Li, and C. Gu, "Broadband and polarization-insensitive absorption based on a set of multisized Fabry-Perot-like resonators," J. Phys. Chem. C **123**, 13856 (2019).
113. Q. Liang, T. Wang, Z. Lu, Q. Sun, Y. Fu, and W. Yu, "Metamaterial-based two dimensional plasmonic subwavelength structures offer the broadest waveband light harvesting," Adv. Opt. Mater. **1**, 43 (2013).
114. T. Chen, M. Yub, Y. Lu, and T. Yen, "Ultra-broadband, lithography-free, omnidirectional, and polarization-insensitive perfect absorber," Sci. Rep. **11**, 5173 (2021).
115. J. Zhao, Y. Wang, Y. Zhu, W. Zhang, and Y. Yu, "Lithography-free, flexible perfect broadband absorber in visible light based on all-dielectric multilayer structure," Opt. Lett. **45**, 5464 (2020).
116. C. Dong, K.-S. Shen, Y. Zheng, H.-C. Liu, J. Zhang, S.-Q. Xia, F. Wu, H. Lu, X.-Z. Zhang, and Y.-F. Liu, "Quasiperiodic metamaterials empowered non-metallic broadband optical absorbers," Opt. Express **29**, 13576 (2021).
117. H. Zhong, H. Zhang, Z. Liu, X. Liu, and G. Liu, "Super-absorbers by randomly distributed titanium spheres," IEEE Photon. Technol. Lett. **33**, 247 (2021).
118. Z. Guo, X. Liu, C. Li, J. Li, H. Cai, M. Fu, D. He, and Y. Wang, "Near-perfect broadband metamaterial absorbers of truncated nanocones using colloidal lithography," Opt. Mater. **119**, 111352 (2021).
119. J. Zhou, X. Liu, H. Zhang, M. Liu, Q. Yi, Z. Liu, and J. Wang, "Cross-shaped titanium resonators based metasurface for ultra-broadband solar absorption," IEEE Photon. J. **13**, 3052990 (2021).
120. Q. Qian, C. Wang, L. Fan, L. Cheng, H. Chen, and L. Zhao, "An ultra-broadband metasurface perfect absorber based on the triple Mie resonances," Opt. Mater. **116**, 111103 (2021).
121. R. Piao and D. Zhang, "Ultra-broadband perfect absorber based on nano-array of titanium nitride truncated pyramids for solar energy harvesting," Physica E Low Dimens. Syst. Nanostruct. **134**, 114829 (2021).
122. H. Zhang, M. Luo, Y. Zhou, Y. Ji, and L. Chen, "Ultra-broadband, polarization-independent, wide-angle near-perfect absorber based on one-dimensional meta-surface from UV to near-infrared region," Opt. Mater. Express **10**, 484 (2020).
123. H. Zhang, L. Feng, Y. Liang, and T. Xu, "An ultra-flexible plasmonic metamaterial film for efficient omnidirectional and broadband optical absorption," Nanoscale **11**, 437 (2019).
124. J. Grant, Y. Ma, S. Saha, A. Khalid, and D. R. Cumming, "Polarization insensitive, broadband terahertz metamaterial absorber," Opt. Lett. **36**, 3476 (2011).
125. D. M. Nguyen, D. Lee, and J. Rho, "Control of light absorbance using plasmonic grating based perfect absorber at visible and near-infrared wavelengths," Sci. Rep. **7**, 2611 (2017).
126. K. Chen, R. Adato, and H. Altug, "Dual-band perfect absorber for multispectral plasmon-enhanced infrared spectroscopy," ACS Nano **6**, 7998 (2012).
127. M. Pu, C. Hu, M. Wang, C. Huang, Z. Zhao, C. Wang, Q. Fang, and X. Luo, "Design principles for infrared wide-angle perfect absorber based on plasmonic structure," Opt. Express **19**, 17413 (2011).

128. C. Han, R. Zhong, Z. Liang, L. Yang, Z. Fang, Y. Wang, A. Ma, Z. Wu, M. Hu, D. Liu, and S. Liu, "Independently tunable multipurpose absorber with single layer of metal-graphene metamaterials," Materials **14**, 284 (2021).
129. Y. Zhao, Q. Huang, H. Cai, X. Lin, H. He, T. Ma, and Y. Lu, "Dual band and tunable perfect absorber based on dual gratings-coupled graphene-dielectric multilayer structures," Opt. Express **27**, 5217 (2019).
130. Y. Zhang, T. Li, Q. Chen, H. Zhang, J. F. O'Hara, E. Abele, A. J. Taylor, H. Chen, and A. K. Azad, "Independently tunable dual-band perfect absorber based on graphene at mid-infrared frequencies," Sci. Rep. **5**, 18463 (2015).
131. X. Han, Y. B. Wu, J. Dong, M. C. Tang, Y. N. Jiang, and X. P. Zeng, "Ultra-thin and broadband tunable metamaterial graphene absorber," Opt. Express **26**, 1681 (2018).
132. M. Wuttig, H. Bhaskaran, and T. Taubner, "Phase-change materials for non-volatile photonic applications," Nat. Photonics **11**, 465 (2017).
133. Q. Y. Wen, H. W. Zhang, Q. H. Yang, Y. S. Xie, K. Chen, and Y. L. Liu, "Terahertz metamaterials with VO_2 cut-wires for thermal tunability," Appl. Phys. Lett. **97**, 021111 (2010).
134. Y. Chen, X. Li, X. Luo, S. Maier, and M. Hong, "Tunable near-infrared plasmonic perfect absorber based on phase-change materials," Photon. Res. **3**, 54 (2015).
135. J. Jeong, A. Joushaghani, S. Paradis, D. Alain, and J. K. S. Poon, "Electrically controllable extraordinary optical transmission in gold gratings on vanadium dioxide," Opt. Lett. **40**, 4408 (2015).
136. L. Wang, E. Radue, S. Kittiwatanakul, C. Clavero, J. Lu, S. A. Wolf, I. Novikova, and R. A. Lukaszew, "Surface plasmon polaritons in VO_2 thin films for tunable low-loss plasmonic applications," Opt. Lett. **37**, 4335 (2012).
137. C. Peng, K. Ou, G. Li, X. Li, W. Wang, Z. Zhao, X. Li, X. Chen, and W. Lu, "Tunable phase change polaritonic perfect absorber in the mid-infrared region," Opt. Express **28**, 11721 (2020).
138. Z. Zheng, Y. Zheng, Y. Luo, Z. Yi, J. Zhang, Z. Liu, W. Yang, Y. Yu, X. Wu, and P. Wu, "A switchable terahertz device combining ultra-wideband absorption and ultra-wideband complete reflection," Phys. Chem. Chem. Phys. **24**, 2527 (2022).
139. Y. Yao, R. Shankar, M. A. Kats, Y. Song, J. Kong, M. Loncar, and F. Capasso, "Electrically tunable metasurface perfect absorbers for ultrathin mid-infrared optical modulators," Nano Lett. **14**, 6526 (2014).
140. Y. Yang, K. Kelley, E. Sachet, S. Campione, T. S. Luk, J.-P. Maria, M. B. Sinclair, and I. Brener, "Femtosecond optical polarization switching using a cadmium oxide-based perfect absorber," Nat. Photonics **11**, 390 (2017).
141. J. He, M. Zhang, S. Shu, Y. Yan, and M. Wang, "VO_2 based dynamic tunable absorber and its application in switchable control and real-time color display in the visible region," Opt. Express **28**, 37590 (2020).
142. D. N. Ma, H. Cheng, J. G. Tian, and S. Q. Chen, "Inverse design methods and applications of photonics devices (Invited)," Acta Photonica Sin. **51**, 0151110 (2022).
143. H. Yu, Y. Peng, Y. Yang, and Z. Y. Li, "Plasmon-enhanced light–matter interactions and applications," NPJ Computat. Mater. **5**, 45 (2019).
144. D. G. Baranov, A. Krasnok, T. Shegai, A. Alu, and Y. D. Chong, "Coherent perfect absorbers: linear control of light with light," Nat. Rev. Mater **2**, 17064 (2017).
145. S. A. Mann and E. C. Garnett, "Resonant nanophotonic spectrum splitting for ultrathin multijunction solar cells," ACS Photonics **2**, 816 (2015).
146. F. Dincer, O. Akgol, M. Karaaslan, E. Unal, and C. Sabah, "Polarization angle independent perfect metamaterial absorbers for solar cell applications in the microwave, infrared, and visible regime," Prog. Electromagn. Res. **144**, 93 (2014).
147. S. M. Kim, J. S. Won, and S. H. Nahm, "Simultaneous reception of solar power and visible light communication using a solar cell," Opt. Eng. **53**, 046103 (2014).
148. P. Rufangura and C. Sabah, "Wide-band polarization independent perfect metamaterial absorber based on concentric rings topology for solar cells application," J. Alloys Compd. **680**, 473 (2016).
149. C. F. Huang, W. Y. Hsieh, B. C. Hsieh, C. H. Hsieh, and C. F. Lin, "Characterization of InGaN-based photovoltaic devices by varying the indium contents," Thin Solid Films **529**, 278 (2013).
150. G. E. Cirlin, A. D. Bouravleuv, I. P. Soshnikov, Y. B. Samsonenko, V. G. Dubrovskii, E. M. Arakcheeva, E. M. Tanklevskaya, and P. Werner, "Photovoltaic properties of p-doped GaAs nanowire arrays grown on n-type GaAs(111)B substrate," Nano. Res. Lett. **5**, 360 (2009).
151. X. Tang, M. M. Ackerman, and P. Guyot-Sionnest, "Thermal imaging with plasmon resonance enhanced HgTe colloidal quantum dot photovoltaic devices," ACS Nano **12**, 7362 (2018).
152. I. A. Hummelgen, "Organic electronic solid state device: electrochemistry of material preparation," J. Solid State Electrochem. **21**, 1977 (2017).
153. S. Mallawaarachchi, M. Premaratne, S. D. Gunapala, and P. K. Maini, "Tuneable superradiant thermal emitter assembly," Phys. Rev. B **95**, 155443 (2017).
154. G. Liu, X. Liu, J. Chen, Y. Li, L. Shi, G. Fu, and Z. Liu, "Near-unity, full-spectrum, nanoscale solar absorbers and near-perfect blackbody emitters," Sol. Energ. Mater. Sol. C **190**, 20 (2019).
155. X. Liu, T. Tyler, T. Starr, A. F. Starr, N. M. Jokerst, and W. J. Padilla, "Taming the blackbody with infrared metamaterials as selective thermal emitters," Phys. Rev. Lett. **107**, 045901 (2011).
156. Y. Nam, Y. Yeng, A. Lenert, P. Bermel, I. Celanovic, M. Soljačić, and E. N. Wang, "Solar thermophotovoltaic energy conversion systems with two-dimensional tantalum photonic crystal absorbers and emitters," Sol. Energ. Mater. Sol. C **122**, 287 (2014).
157. Y. Li, X. Bai, D. Yuan, F. Zhang, B. Li, X. San, B. Liang, S. Wang, J. Luo, and G. Fu, "General heterostructure strategy of photothermal materials for scalable solar-heating hydrogen production without the consumption of artificial energy," Nat. Commun. **13**, 776 (2022).
158. Z. H. Liu, H. Y. Guan, and G. S. Wang, "Performance optimization study on an integrated solar desalination system with multi-stage evaporation/heat recovery processes," Energy **76**, 1001 (2014).
159. Z. H. Liu, R. L. Hu, and X. J. Chen, "A novel integrated solar desalination system with multi-stage evaporation/heat recovery processes," Renew. Energy **64**, 26 (2014).
160. S. F. Li, Z. H. Liu, Z. X. Shao, H. S. Xiao, and N. Xia, "Performance study on a passive solar seawater desalination system using multi-effect heat recovery," Appl. Energy **213**, 343 (2018).
161. L. Zhou, S. D. Zhuang, C. Y. He, Y. L. Tan, Z. L. Wang, and J. Zhu, "Self-assembled spectrum selective plasmonic absorbers with tunable bandwidth for solar energy conversion," Nano Energy **32**, 195 (2017).
162. L. Li, Y. Liu, P. Hao, Z. Wang, L. Fu, Z. Ma, and J. Zhou, "PEDOT nanocomposites mediated dual-modal photodynamic and photothermal targeted sterilization in both NIR I and II window," Biomaterials **41**, 132 (2015).
163. S. Pirnat, M. Lukac, and A. Ihan, "Study of the direct bactericidal effect of Nd:YAG and diode laser parameters used in endodontics on pigmented and nonpigmented bacteria," Lasers Med. Sci. **26**, 755 (2011).
164. W. H. Wang, H. B. Wang, P. Yu, K. Sun, X. Tong, F. Lin, C. Wu, Y. M. You, W. Z. Xie, Y. P. Li, C. Z. Yuan, A. O. Govorov, O. L. Muskens, H. X. Xu, S. Sun, and Z. M. Wang, "Broadband thin-film and metamaterial absorbers using refractory vanadium nitride and their thermal stability," Opt. Express **29**, 33456 (2021).
165. K. Aydin, V. E. Ferry, R. M. Briggs, and H. A. Atwater, "Broadband polarization-independent resonant light absorption using ultrathin plasmonic super absorbers," Nat. Commun. **2**, 517 (2011).
166. Z. Li, S. Butun, and K. Aydin, "Lithography-free transmission filters at ultraviolet frequencies using ultra-thin aluminum films," J. Opt. **18**, 065006 (2016).
167. R. Yang, C. Dai, C. Wan, G. Zheng, and Z. Li, "Planar ultrathin omni-directional perfect absorber utilizing amorphous silicon for photovoltaics," Opt. Mater. Express **10**, 532 (2020).
168. B. Wang, E. Stevens, and P. W. Leu, "Strong broadband absorption in GaAs nanocone and nanowire arrays for solar cells," Opt. Express **22**, A386 (2014).
169. I. Massiot, N. Vandamme, N. Bardou, C. Dupuis, A. Lemaître, J. F. Guillemoles, and S. Collin, "Metal nanogrid for broadband multiresonant light-harvesting in ultrathin GaAs layers," ACS Photonics **1**, 878 (2014).
170. Y. Li, X. Yan, Y. Wu, X. Zhang, and X. Ren, "Plasmon-enhanced light absorption in GaAs nanowire array solar cells," Nanoscale Res. Lett. **10**, 436 (2015).

171. X. L. Lin, C. W. Hsu, and G. P. Wang, "Frequency-selective omnidirectional scattering of light by weakly disordered periodic planar arrays of dielectric particles," Opt. Express **24**, 23136 (2016).
172. Z. Wang, G. Duan, and H. Duan, "Optimization of the perfect absorber for solar energy harvesting based on the cone-like nanostructures," AIMS Energy **9**, 714 (2021).
173. M. K. Hedayati, M. Javaherirahim, B. Mozooni, R. Abdelaziz, A. Tavassolizadeh, V. S. Kiran Chakravadhanula, V. Zaporojtchenko, T. Strunkus, F. Faupel, and M. Elbahri, "Design of a perfect black absorber at visible frequencies using plasmonic metamaterials," Adv. Mater. **23**, 5410 (2011).
174. A. Moreau, C. Ciracì, J. J. Mock, R. T. Hill, Q. Wang, B. J. Wiley, A. Chilkoti, and D. R. Smith, "Controlled-reflectance surfaces with film-coupled colloidal nanoantennas," Nature **492**, 86 (2012).
175. T. Reininger, F. Welker, and M. V. Zeppelin, "Sensors in position control applications for industrial automation," Sens. Actuat. A: Phys. **129**, 270 (2006).
176. M. Indri, L. Lachello, I. Lazzero, F. Sibona, and S. Trapani, "Smart sensors applications for a new paradigm of a production line," Sensors **19**, 650 (2019).
177. K. Minoglou, N. Nelms, A. Ciapponi, H. Werber, S. Wittig, B. Leone, and P. E. Crouzet, "Infrared image sensor developments supported by the European space agency," Infrared Phys. Technol. **96**, 351 (2019).
178. C. Liu, J. Lü, W. Liu, F. Wang, and P. K. Chu, "Overview of refractive index sensors comprising photonic crystal fibers based on the surface plasmon resonance effect [Invited]," Chin. Opt. Lett. **19**, 102202 (2021).
179. H. H. Cho, T. K. Shih, and H. C. Chao, "A robust coverage scheme for UWSNs using the spline function," IEEE Sens. J. **16**, 3995 (2016).
180. J. Aguzzi, M. M. Flexas, S. Flögel, C. Lo Iacono, M. Tangherlin, C. Costa, S. Marin, N. Bahamon, S. Martin, E. Fanell, R. Danovaro, S. Stefann, L. Thomsen, G. Riccobene, M. Hildebrand, I. Masmitja, J. Del Rio, E. B. Clark, A. Branch, P. Weiss, A. T. Klesh, and M. P. Schodlok, "Exo-ocean exploration with deep-sea sensor and platform technologies," Astrobiology **20**, 897 (2020).
181. Z. Bielecki, T. Stacewicz, J. Wojtas, J. Mikołajczyk, D. Szabra, and A. Prokopiuk, "Selected optoelectronic sensors in medical applications," Opto-Electron. Rev. **26**, 122 (2018).
182. Y. Zhu, D. Liu, R. Grosu, X. Wang, H. Duan, and G. Wang, "A multi-sensor data fusion approach for atrial hypertrophy disease diagnosis based on characterized support vector hyperspheres," Sensors **17**, 2049 (2017).
183. S. T. Han, H. Peng, Q. Sun, S. Venkatesh, K. S. Chung, S. C. Lau, Y. Zhou, and V. A. L. Roy, "An overview of the development of flexible sensors," Adv. Mater. **29**, 1700244 (2017).
184. J. Chen, H. Nie, C. J. Tang, Y. H. Cui, B. Yan, Z. Y. Zhang, Y. R. Kong, Z. J. Xu, and P. G. Cai, "Highly sensitive refractive-index sensor based on strong magnetic resonance in metamaterials," Appl. Phys. Express **12**, 052015 (2019).
185. N. Liu, M. Mesch, T. Weiss, M. Hentschel, and H. Giessen, "Infrared perfect absorber and its application as plasmonic sensor," Nano lett. **10**, 2342 (2010).
186. Z. L. Deng, T. Fu, Z. B. Ouyang, and G. P. Wang, "Trimeric metasurfaces for independent control of bright and dark modes of Fano resonances," Appl. Phys. Lett. **108**, 081109 (2016).
187. Z. Shen and M. Du, "High-performance refractive index sensing system based on multiple Fano resonances in polarization-insensitive metasurface with nanorings," Opt. Express **29**, 28287 (2021).
188. N. Uddin, G. Q. Du, F. Chen, Y. Lu, Q. Yang, H. Bian, J. L. Yong, and X. Hou, "Fano resonance-assisted plasmonic trapping of nanoparticles," Plasmonics **12**, 627 (2017).
189. J. Y. Jung, J. Lee, J. H. Choi, D. G. Choi, and J. H. Jeong, "Enhancement of refractive index sensing for an infrared plasmonic metamaterial absorber with a nanogap," Opt. Express **29**, 22796 (2021).
190. Z. Yan, Q. Zhu, M. Wan, X. Lu, X. Pu, C. Tang, and L. Yu, "Graphene ultraviolet ultrahigh-*Q* perfect absorption for nanoscale optical sensing," Opt. Express **28**, 6095 (2020).
191. Z. Yan, X. Lu, W. Du, Z. Lv, C. Tang, P. Cai, P. Gu, J. Chen, and Z. Yu, "Ultraviolet graphene ultranarrow absorption engineered by lattice plasmon resonance," Nanotechnology **32**, 465202 (2021).
192. Y. H. Xian, Y. Cai, X. Y. Sun, X. F. Liu, Q. B. Guo, Z. X. Zhang, L. M. Tong, and J. R. Qiu, "Refractory plasmonic metal nitride nanoparticles for broadband near-infrared optical switches," Laser Photonics Rev. **13**, 1900029 (2019).
193. S. L. Li, M. H. Yuan, W. J. Zhuang, X. Zhao, S. L. Tie, J. Xiang, and S. Lan, "Optically-controlled quantum size effect in a hybrid nanocavity composed of a perovskite nanoparticle and a thin gold film," Laser Photonics Rev. **15**, 2000480 (2021).
194. X. W. Jiang, S. Wang, and H. Wu, "Metamaterial absorber with tunable absorption bandwidth based on vanadium dioxide," Acta Photonica Sin. **51**, 0151124 (2022).
195. X. Liu, G. Liu, P. Tang, G. Fu, G. Du, Q. Chen, and Z. Liu, "Quantitatively optical and electrical-adjusting high-performance switch by graphene plasmonic perfect absorbers," Carbon **140**, 362 (2018).
196. Z. Q. Liu, J. Zhou, X. S. Liu, G. L. Fu, G. Q. Liu, C. J. Tang, and J. Chen, "High-*Q* plasmonic graphene absorbers for electrical switching and optical detection," Carbon **166**, 256 (2020).
197. X. M. Du, F. P. Yan, W. Wang, L. N. Zhang, Z. Y. Bai, H. Zhou, and Y. F. Hou, "A broadband switchable metamaterial absorber/reflector based on multi-laps graphene sheets in the terahertz band," IEEE Photonics J. **13**, 4600208 (2021).
198. Y. B. Zhang, H. Liu, H. Cheng, J. G. Tian, and S. Q. Chen, "Multidimensional manipulation of wave fields based on artificial microstructures," Opto-Electron. Adv. **3**, 200002 (2020).
199. Y. Shi, X. Chen, F. Lou, Y. Chen, M. Yan, L. Wosinski, and M. Qiu, "All-optical switching of silicon disk resonator based on photothermal effect in metal-insulator-metal absorber," Opt. Lett. **39**, 4431 (2014).
200. Z. H. Han and Y. J. Cai, "All-optical self-switching with ultralow incident laser intensity assisted by a bound state in the continuum," Opt. Lett. **46**, 524 (2021).
201. S. W. Yu, Z. C. Li, W. W. Liu, H. Cheng, Y. B. Zhang, B. Y. Xie, W. Y. Zhou, J. G. Tian, and S. Q. Chen, "Tunable dual-band and high-quality-factor perfect absorption based on VO_2-assisted metasurfaces," Opt. Express **29**, 31488 (2021).
202. B. Zeng, Z. Huang, A. Singh, Y. Yao, A. K. Azad, A. D. Mohite, A. J. Taylor, D. R. Smith, and H. Chen, "Hybrid graphene metasurfaces for high-speed mid-infrared light modulation and single-pixel imaging," Light Sci. Appl. **7**, 51 (2018).
203. C. Pang, R. Li, Y. Zhang, Z. Li, N. Dong, L. Wu, H. Yu, J. Wang, F. Ren, and F. Chen, "Tailoring optical nonlinearities of $LiNbO_3$ crystals by plasmonic silver nanoparticles for broadband saturable absorbers," Opt. Express **26**, 31276 (2018).
204. L. Zhao, F. Cai, L. Tong, Y. Yuan, W. Zhang, and Y. Cai, "Theoretical analysis of periodically poled $LiNbO_3$ nonlinear mirror and its application in a passively mode-locked Nd:YSAG laser," Chin. Opt. Lett. **19**, 091403 (2021).
205. B. Zhang, L. Wang, and F. Chen, "Recent advances in femtosecond laser processing of $LiNbO_3$ crystals for photonic applications," Laser Photonics Rev. **14**, 1900407 (2020).
206. Y. Tang, Y. Chen, H. Jiang, and X. Chen, "Proposal of switchable multiwavelength laser with continuously tunable spacing in MgO:APPLN waveguide," Chin. Opt. Lett. **11**, 071301 (2013).
207. G. Liu, Q. Wu, X. Liu, X. Zhan, G. Fu, C. Tang, and Z. Liu, "High-performance electro-optic manipulation by plasmonic light absorber with nano-cavity field confinement," IEEE Photonics J. **13**, 4600309 (2021).
208. Y. Jia, L. Wang, and F. Chen, "Ion-cut lithium niobate on insulator technology: recent advances and perspectives," Appl. Phys. Rev. **8**, 011307 (2021).
209. N. Muhammad, Z. Ouyang, X. Tang, and Q. Liu, "Broadband wide-angle incident light absorption by metallic loop metasurfaces based on electro-optic substrate," IEEE Photon. Tech. Lett. **31**, 1068 (2019).
210. X. Zhu, W. Yan, U. Levy, N. A. Mortensen, and A. Kristensen, "Resonant laser printing of structural colors on high-index dielectric metasurfaces," Sci. Adv. **3**, e1602487 (2017).
211. P. Hosseini, C. D. Wright, and H. Bhaskaran, "An optoelectronic framework enabled by low-dimensional phase-change films," Nature **511**, 206 (2014).
212. S. Yokogawa, S. P. Burgos, and H. A. Atwater, "Plasmonic color filters for CMOS image sensor applications," Nano Lett. **12**, 4349 (2012).

213. A. Tittl, A. K. U. Michel, M. Schäferling, X. Yin, B. Gholipour, L. Cui, M. Wuttig, T. Taubner, F. Neubrech, and H. Giessen, "A switchable mid-infrared plasmonic perfect absorber with multispectral thermal imaging capability," Adv. Mater. **27**, 4597 (2015).
214. J. Guo, C. M. Huard, Y. Yang, Y. J. Shin, K. T. Lee, and L. J. Guo, "ITO-free, compact, color liquid crystal devices using integrated structural color filters and graphene electrodes," Adv. Opt. Mater. **2**, 435 (2014).
215. H. Liu, H. Yang, Y. Li, B. Song, Y. Wang, Z. Liu, L. Peng, H. Lim, J. Yoon, and W. Wu, "Switchable all-dielectric metasurfaces for full-color reflective display," Adv. Opt. Mater. **7**, 1801639 (2019).
216. C. S. Park and S. S. Lee, "Vivid coloration and broadband perfect absorption based on asymmetric Fabry–Pérot nanocavities incorporating platinum," ACS Appl. Nano Mater. **4**, 4216 (2021).
217. J. C. Zhao, Y. Zhou, Y. H. Huo, B. Gao, Y. G. Ma, and Y. T. Yu, "Flexible dynamic structural color based on an ultrathin asymmetric Fabry-Perot cavity with phase-change material for temperature perception," Opt. Express **29**, 23273 (2021).
218. G. H. Rui, C. C. Ding, B. Gu, Q. Q. Gan, Q. W. Zhan, and Y. P. Cui, "Symmetric $Ge_2Sb_2Te_5$ based metamaterial absorber induced dynamic wide-gamut structural color," J. Opt. **22**, 085003 (2020).